Regionalized protein localization domains in the hair cell kinocilium.

Timothy Erickson [1, *], William Paul Biggers III [2], Kevin Williams [2], Shyanne E. Butland [1], and Alexandra Venuto [2]

[1] Department of Biology, University of New Brunswick, Fredericton, NB E3B 5A3, Canada

[2] Department of Biology, East Carolina University, Greenville, NC 27858, USA

*Correspondence: timothy.erickson@unb.ca

Abstract:

Sensory hair cells are the receptors for auditory, vestibular, and lateral line sensory organs in vertebrates. These cells are distinguished by "hair"-like projections from their apical surface collectively known as the hair bundle. Along with the staircase arrangement of actin-filled stereocilia, the hair bundle features a single, non-motile, true cilium called the kinocilium. The kinocilium plays important roles in hair bundle development and the mechanics of sensory detection. To understand more about kinocilial development and structure, we performed a transcriptomic analysis of zebrafish hair cells looking for cilia-associated genes that have yet to be characterized in hair cells. Here, we focus on three such genes - *ankef1a*, *odf3l2a*, and *saxo2* - because the human or mouse orthologs are either associated with sensorineural hearing loss or are located near uncharacterized deafness loci. We made transgenic fish that express fluorescently tagged versions of their proteins, demonstrating their localization to the kinocilia of zebrafish hair cells. Furthermore, we find that Ankef1a, Odf3l2a, and Saxo2 exhibit distinct localization patterns along the length of the kinocilium. Lastly, we report a novel overexpression phenotype for Saxo2. Overall, these results suggest that the hair cell kinocilium is regionalized along its proximal-distal axis and set the groundwork to understand more about the roles of these kinocilial proteins in hair cells.

Keywords:

hair cells; kinocilium; cilia; deafness; hearing loss; lateral line; transcriptomics; TU-tagging; zebrafish; ANKEF1; ODF3L2; SAXO2

1. Introduction

Our senses of hearing and balance rely on the function of sensory receptors in our ears called hair cells. Sensory hair cells are distinguished by hair-like projections from their apical surface that detect and transduce physical stimuli such as sound waves or head movements. Most of these projections are actin-filled microvilli (called stereocilia) that form the characteristic stair-cased hair bundle. However, at some point in their development, all vertebrate hair cells also feature a single microtubule-based projection called the kinocilium.

Cilia play prominent roles in sensory cell development and function from an evolutionarily diverse set of organisms [1,2]. In mechanosensory hair cells, the kinocilium can fulfil both sensory and structural roles, depending on the type of hair cell. Although kinocilia degenerate around the onset of hearing in mammalian cochlear hair cells, they nonetheless play a developmental role in establishing hair bundle polarity in the auditory system [3] and mediating Sonic Hedgehog signaling to instruct cochlear development [4,5]. In contrast to the transient kinocilia of cochlear hair cells, the kinocilium is a permanent and prominent feature of most other vertebrate hair cells in the auditory, vestibular, and lateral line organs, including vestibular hair cells of mammals. In non-cochlear cells, it appears that kinocilia play a less pronounced role in establishing bundle polarity. However, they contribute to the structure and functional mechanics of the sensory hair bundle [6–8], as well as act as attachment points for inert masses such as otoliths and otoconia [9]. Kinocilial dynamics may also be involved in the repair and regeneration of cochlear hair cells [10]. As such, characterizing functional components of the kinocilium is fundamental to our understanding of sensory hair cells.

Hair cell kinocilia possess several features that distinguish them from both non-motile, primary cilia and from motile cilia and flagella. Although "kino-" means "motion" and kinocilia usually possess the "9+2" arrangement of axonemal microtubules typically found in motile cilia [11], the hair cell cilium is non-motile, lacking the inner dynein arms and nexin links found in motile cilia [12]. In this respect, kinocilia are similar to some mammalian olfactory cilia, which also have a 9+2 axoneme but lack the dynein machinery to generate motion [13]. However, given the impressive diversity of vertebrate hair cells, it is possible that active movement is a feature of some kinocilia [14,15]. In some contexts, non-"9+2" arrangements of microtubules have also been reported [10,12]. Like hair cells themselves, there is great diversity in kinocilial morphology - from the transient kinocilia of cochlear hair cells, to the bulbed kinocilia of amphibian hair cells, to the towering kinocilia of superficial lateral line neuromasts (and everything in between). However, little is known about the molecular bases for this diversity.

Sensorineural hearing loss can result from mutations in cilia-associated genes as part of a syndromic ciliopathy, such as reported for Alström, Bardet-Biedl, and Usher syndromes [16–18]. Cilia- and microtubule associated genes are also implicated in nonsyndromic hearing loss, examples being *CCDC50* [19], *MAP1B* [20], and *DCDC2* [21]. *PCDH15* and *CDH23* are also examples of cilia-associated Usher proteins where certain alleles result in nonsyndromic hearing loss [22,23]. There may be other cilia-associated genes waiting to be identified that contribute to auditory and / or vestibular function.

To characterize putative kinocilial genes, we have turned to the zebrafish model system. Zebrafish hair cells are genetically and molecularly related to mammalian hair cells [24]. This allows us to utilize the genetic tractability of zebrafish to characterize protein localization and function for putative human deafness genes. Here, we identify hair cell-enriched transcripts by TU-tagging and focus on three putative kinocilial genes within the dataset - *ankef1a*, *odf3l2a*, and *saxo2* - because of their potential involvement in hearing loss. Mouse *Ankef1* lies within the coloboma (*Cm*) deletion locus whose phenotypes include auditory and vestibular deficits [25,26]. The Shared Harvard Inner Ear Database (SHIELD) reports that human *ODF3L2* and *SAXO2* lie within deafness loci DFNB72 and DFNA30, respectively [27]. We have made transgenic fish that express tagged Ankef1a, Odf3l2a, and Saxo2 proteins and demonstrate their distinct localization patterns within the kinocilium of zebrafish hair cells. Our results set the groundwork for future studies to understand the role of these kinocilial proteins in hair cell structure and function.

2. Methods

2.1. Animal husbandry

Adult zebrafish were maintained and bred using standard procedures [28]. Larval fish were grown at 28.5ºC on a 14:10 hour light cycle in 100 mm Petri dishes containing E3 media (5 mM NaCl, 0.17 mM KCl, 0.33 mM CaCl2 and 0.33 mM MgSO4 buffered with NaHCO3).

2.2. Transgenic fish lines

The *Tg(myo6b:actb1-EGFP)vo8* and *Tg(myo6b:yfp-Hsa.TUBA)idc16* transgenic lines have been previously described [8,29] and were gifts from the lab of Teresa Nicolson. For the TU-tagging experiments, we used a *Tg(myo6b:HA-UPRT-P2A-NLS-mCherry)* line that was similar to, but distinct from, the *Tg(HA-UPRT-P2A-mCherry)* line used previously [30]. The *Tg(myo6b:ankef1a-emGFP)unb4*, *Tg(myo6b:odf3l2a-emGFP)unb5*, *Tg(myo6b:saxo2-emGFP)unb6*, and *Tg(myo6b:saxo2-mKate2)unb7* lines were generated for this study. For the sake of simplicity, we refer to these lines as Ankef1a-GFP, Odf3l2a-GFP, Saxo2-GFP, and Saxo2-mKate2 throughout the manuscript. Coding sequences were amplified using total RNA from 7 days post-fertilization (dpf) zebrafish using the SuperScript IV One-step RT-PCR kit (ThermoFisher) using the primers listed in Table S1. Entry and Destination constructs were made using standard Tol2 Gateway cloning protocols [31].

2.3. Thiouracil (TU)-tagging and bioinformatics

TU-tagging experiments were performed essentially as previously described [30] with the following modifications. Transgenic and wild type sibling larvae from outcrosses of a *Tg(myo6b:HA-UPRT-P2A-NLS-mCherry)* (abbreviated *Tg(UPRT)*) line were used. Stock solutions of 4-thiouracil (4TU; Sigma-Aldrich 440736) and 4-thiouridine (4sU; Sigma-Aldrich T4509) were prepared at 0.5 M and 0.25 M, respectively in DMSO (Sigma-Aldrich D8418). Working solutions were diluted in E3 media with a final DMSO concentration of 0.5%. At 4 dpf, *Tg(UPRT)* larvae were treated with 2 mM 4TU while non-transgenic siblings were treated with 1 mM 4sU. Both groups were bathed in their respective compounds for 3.5 hours at 29ºC. Conversion of 4TU to 4-thiouridine monophosphate is enhanced in the presence of the *Toxoplasma gondii* UPRT enzyme while

117 endogenous biosynthetic pathways can make 4-thiouridine monophosphate directly from
118 4sU. With this strategy, TU-tagged RNA is preferentially synthesized in the hair cells of
119 *Tg(UPRT)* larvae treated with 4TU while RNA is tagged without bias for cell type in 4sU-
120 treated, non-transgenic controls. The experiment was performed in biological replicate
121 where a biological sample is defined as 100 larvae per treatment group produced by a single
122 breeding event.

123 Samples were processed in TRIzol reagent (Ambion 15596026) according to the
124 manufacturer's protocol and enriched for polyadenylated mRNA using the Dynabeads
125 Oligo(dT)25 kit (Ambion 61005). Biotinylation of the mRNA was done using the MTSEA-
126 biotin-XX reagent (Biotium 90066). A 5 mg/ml solution was prepared in *N,N*-
127 Dimethylformamide (DMF; Sigma-Aldrich 227056). A 10X biotinylation buffer was
128 prepared by diluting 1 M Tris-HCl pH 7.5 (ThermoFisher 15567027) to 100 mM and 0.5
129 M EDTA pH 8 (ThermoFisher AM9261) to 10 mM in nuclease-free water (ThermoFisher
130 AM9930). The biotinylation reaction was performed by heating the mRNA in a 1X
131 biotinylation buffer solution at 65ºC for 2 minutes before adding 10 µg of MTSEA-biotin-
132 XX solution with a final DMF concentration of 25%. Samples were incubated in the dark
133 at room temperature for 30 minutes on a rotating rack. mRNA was recovered by adding an
134 equal volume of chloroform:isoamyl alcohol 24:1 (Sigma-Aldrich C0549), vortexing,
135 retrieving the aqueous phase with 5Prime Phase Lock Gel (Heavy) microfuge tubes, and
136 performing a NaCl-isopropanol precipitation with glycogen (ThermoFisher R0551) acting
137 as an inert carrier. Biotinylated RNA was fragmented to approximately 200 – 500 bases
138 with the NEBNext Magnesium RNA Fragmentation Module (New England Biolabs
139 E6150S) and precipitated by adding 1/10 volume of 3M sodium acetate pH 5.5
140 (ThermoFisher AM9740) plus 3 volumes of 100% ethanol, again with glycogen as an inert
141 carrier. Finally, biotinylated TU-tagged RNA was separated from untagged RNA using the
142 µMacs Streptavidin kit (Miltenyi Biotec 130-074-101). High salt MPG buffer (100 mM
143 Tris, 10 mM EDTA, 1 M NaCl, 0.1% Tween-20) and 100 mM dithiothreitol (DTT; Sigma-
144 Aldrich 3860-OP) were prepared fresh. RNA samples (50 ul) were heated to 65ºC for 5
145 minutes and iced. Resuspended µMass beads (100 µl) were added and samples were
146 incubated for 15 minutes in the dark at room temperature with rotation. µMacs columns
147 were equilibrated with 2 x 100 µl of nucleic acid buffer (supplied with kit) before applying
148 the RNA-bead samples to the columns. Columns were washed with twice with 65ºC MPG
149 buffer and twice with room temperature buffer. TU-tagged RNA was eluted from each
150 column with 2 x 100 µl 100 mM DTT heated to 65 ºC. Eluted RNA was recovered by
151 NaOAc - ethanol precipitation as above, resulting in two biological samples of hair cell
152 enriched, TU-tagged RNA from *Tg(UPRT)* larvae treated with 4TU and two biological
153 samples of tagged RNA from non-transgenic larvae treated with 4sU.

154 RNA-seq library construction and sequencing was done by the OHSU Massively
155 Parallel Sequencing Shared Resource (Oregon Health & Science University, Portland OR).
156 The raw RNA-seq data was imported into an OHSU instance of the Galaxy platform [32]
157 and mapped to the *Danio rerio* GRCz10 genome. The resulting BAM files were imported
158 to SeqMonk (https://www.bioinformatics.babraham.ac.uk/projects/seqmonk/) for data
159 visualization and statistical analysis using default parameters for DESeq2. Transcripts that
160 were significantly enriched in the *Tg(UPRT)* samples were analyzed for GO biological
161 process term enrichment using the Panther database [33,34]. Analysis of *ODF3L2* and
162 *SAXO2* genomic positions relative to known deafness loci was done using information from

the Hereditary Hearing Loss website [35] and by searching the GRCh38.p13 human genome assembly through Ensembl [36] for the loci-defining genetic markers described in the relevant publications (Table 1).

2.4. Whole mount mRNA in situ hybridization

mRNA in situ hybridizations for *ankef1a*, *odf3l2a,* and *saxo2* were performed as described [30]. Probe templates were amplified using primers listed in Table S1. The *odf3l2a* template was amplified from total RNA with T3 and T7 sites on the forward and reverse primers respectively and the DIG-labeled antisense probe was synthesized directly from purified PCR product using T7 RNA polymerase (NEB M0251S). The *ankef1a* and *saxo2* probe templates were amplified from total RNA with gene specific primers and cloned into the pCR4-TOPO vector (Thermo Fisher 450071). DIG-labeled antisense probes for *ankef1a* and *saxo2* were synthesized with the appropriate RNA polymerase from linearized plasmids (*ankef1a*: NotI, T3 (M0378S); *saxo2*: PmeI, T7).

2.5. Confocal microscopy, image analysis, and statistics

Live zebrafish larvae (5-7 dpf) were anesthetized in 0.016% MS-222 and mounted in 1.2% low-melting point agarose overlaid with E3 media containing MS-222. Confocal imaging was performed with a Zeiss LSM 700 confocal microscope equipped with a 40X water immersion objective. Pixel intensity and kinocilium length analyses were done in Fiji [37] and the "cool" lookup table was used to encode pixel intensity in maximum Z-projections. Neuromast images in Figure 2E-H contain "choppiness" artifacts produced by rotation of 3D Z-projections. Images were compiled and adjusted for brightness and contrast in Adobe Photoshop CC.

Length measurements for lateral cristae kinocilia were done by tracing a kinocilium from base to tip through a confocal Z-stack using the SNT plugin for ImageJ [38,39] and calculating the Euclidean distance for kinocilial length by Pythagorean theorem. The transmitted light channel was used to define the start and end of each kinocilium. A single biological sample (n) is defined as the per larva average of the five tallest kinocilia that could be unambiguously traced. Per larva averages were used for statistical comparisons between transgenic larvae and non-transgenic siblings.

Fluorescent protein distributions along the length of lateral crista kinocilia were quantified in ImageJ using the "plot profile" function with a segmented line width setting of "2". 16-bit pixel intensity values were recorded every 0.064 µm. Measurable kinocilia were defined as having a minimum length of 32 µm and for which the intensity profile could be unambiguously measured from base to distal tip using the transmitted light channel as a guide. To account for differences in kinocilial length, pixel intensity values were registered to the most distal measurement of each kinocilium, meaning that proximal intensity values for kinocilia that are longer than 32 µm are not included in the intensity profile measurement analysis. Pixel intensity values at each position were averaged from all measured kinocilia to create an average gray value over a distance of 32 µm. To account for differences in overall fluorescence levels between transgenes, the average gray values were rescaled using min-max normalization to a 0-100 scale and plotted as log2 values fit with a loess curve.

RNA sequencing data were visualized and plotted using Seqmonk (https://www.bioinformatics.babraham.ac.uk/projects/seqmonk/) and analyzed using

207 default Seqmonk settings for DESeq2. Statistical tests for kinocilial length were performed
208 in R Studio [40] using the base R stats package [41] for Welch two-sided t-tests and the
209 ANOVA. Plots were generated with ggplot2 [42].

210 3. Results

211 *3.1. Identification of putative kinocilia-associated, hair cell-enriched transcripts.*

212 Thiouracil (TU) tagging is a method for purifying mRNA transcripts from specific
213 cell types [43]. To identify genes expressed in sensory hair cells (Figure 1A), we performed
214 TU-tagged RNA-seq experiments on larval zebrafish, introducing several protocol changes
215 relative to our previous study (See Methods) [30]. We identified 1838 features that were
216 significantly enriched in the 4TU-treated *Tg(UPRT)* sample vs. the 4sU-treated wild type
217 controls (Figure 1B). See Table S2 for the full list of significantly TU-enriched genes from
218 this study. Gene Ontology (GO) enrichment analysis of 1675 uniquely mapped features
219 reveals that genes associated with hearing, hair cells, and inner ear development are
220 statistically overrepresented in the TU-enriched dataset (Table S3), confirming that the
221 experiment successfully enriched for hair cell transcripts. There is also a significant
222 enrichment of genes associated with microtubule-and cilium-based processes (Table S4),
223 highlighting genes with potential roles in the structure and / or function of kinocilia.

224 Next, we manually searched the entire TU-enriched dataset for putative kinocilial
225 genes that may be associated with deafness phenotypes in mice and humans, but whose
226 protein products have not been previously localized to the kinocilium. For this study, we
227 focus on three such genes - *ankef1a*, *odf3l2a*, and *saxo2*. Enriched hair cell expression for
228 all three genes was confirmed by mRNA in situ hybridization on 3 days post-fertilization
229 (dpf) larvae. *ankef1a* is primarily expressed in inner ear and lateral line hair cells (Figure
230 1C). This restricted pattern differs from a previous study where *ankef1a* was shown to be
231 more broadly expressed [44]. *odf3l2a* expression is restricted to inner ear and lateral line
232 hair cells (Figure 1D), consistent with the pattern reported for the *et10.4* enhancer trap line
233 where the transgenic insertion is 1.5 kilobases (kb) upstream of the *odf3l2a* gene [45]. *saxo2*
234 is also expressed in otic and lateral line hair cells, with additional robust expression in the
235 developing olfactory epithelia (Figure 1E).

236 *3.2. Evaluation of ANKEF1, ODF3L2, and SAXO2 as potential human deafness genes.*

237 Ankyrin repeat and EF-hand domain containing 1 (ANKEF1) is predicted to contain
238 protein-protein interaction (ankyrin) and calcium-sensing/binding (EF-hand) domains.
239 Functionally, *Ankef1* has been implicated in *Xenopus* gastrulation and fertility in male mice
240 [46,47]. ANKEF1 protein localization to the cilium has not been demonstrated, but
241 transcriptomic and proteomic analyses suggest it is enriched in ciliated cells (including
242 mouse and zebrafish hair cells) [44,48–55].

243 Human *ANKEF1* is on chromosome 20 (GRCh38: 20:10034987-10058303) and not
244 located near any known human deafness loci [35] (Table 1). However, the mouse *Ankef1*
245 ortholog is located within the coloboma (*Cm*) deletion locus [56,57]. *Cm* heterozygotes
246 exhibit morphological abnormalities in the organ of Corti and head bobbing indicative of
247 vestibular defects [26,58]. Most of these *Cm* phenotypes can be attributed to the
248 heterozygous loss of the Notch ligand Jagged 1 (*Jag1*). However, the authors note that the

Cm and *Jag1* mutant phenotypes are not equivalent and speculate that other genes within deletion may contribute to the inner ear defects in *Cm* mutants [26].

Outer dense fiber protein 3-like 2 (ODF3L2) is a member of the ODF3 family of proteins which are characterized by sperm-tail PG (proline-glycine)-rich (STPGR) repeat domains. Note that although ODF families 1-4 share a common nomenclature and associate with microtubule-based structures, these four ODF families are not evolutionarily related to one another. ODF3 (SHIPPO1) was first identified as a component of the outer dense fibers (ODFs) of mouse sperm tails [59]. However, *Odf3* family genes are also expressed in ciliated cells that lack outer dense fibers [60–63], suggesting a broader role in microtubule-based structures [64]. Consistent with this idea, an Odf3l2 homolog in *Giardia* forms part of the basal body proteome [65] and human ODF3L2 can localize to cytoplasmic microtubules in a heterologous expression system [66]. However, ODF3L2 localization to the cilium has not been demonstrated. Functionally, little is known about ODF3 and ODF3L proteins in any cell type. Zebrafish *odf3l2a* is a hair cell-enriched transcript [55] and, although evidence for *Odf3l2* expression in mammalian hair cells is weak, *Odf3l2* knockout mice display high frequency hearing loss and vestibular dysfunction [67]. The underlying cellular causes for these phenotypes are unknown.

Human *ODF3L2* is located on chromosome 19p13.3 (GRCh38:19:463346-474880) (Table 1). The 19p13 region is home to several hearing loss loci, including *DFNB15*/*72*/*95* (*GIPC3*) [68,69], *DFNB68* (*S1PR2*) [70], *DFNB81* / Perrault syndrome (*CLPP*) [68,71], as well as the autosomal dominant *DNFA57* locus (gene unknown) [72]. The *DFNB72* critical region was mapped between markers D19S216 and D19S1034 (GRCh38:19:4949401-6113471) [73]. Although the Shared Harvard Inner-Ear Database (SHIELD) [27] reports that *ODF3L2* is located within the *DFNB72* critical region, the GRCh38 human genome assembly places *ODF3L2* at least 4.4 MB away from the closest *DFNB72* marker D19S216. The *DFNA57* critical region was mapped between markers D19S912 and D19S212 (GRCh38:19:7806762:18232460). *ODF3L2* is almost 7 MB away from the closest marker D19S592 and over 9 MB away from the maximum LOD score marker D19S586. However, the telomeric boundary was defined from a single patient and the authors acknowledge an unlikely possibility that the *DFNA57* interval extends to the telomere. If this is the case, *ODF3L2* remains as a candidate gene for *DFNA57*.

Stabilizer of axonemal microtubules 2 (SAXO2 / FAM154B) is the second of two SAXO family members that are part of the microtubule associated protein 6 (MAP6) family [74,75]. SAXO proteins can stabilize microtubules and use their "Mn" repeat domains to associate with basal bodies, centrioles, and cilia [75–78]. Interestingly, SAXO and MAP6 are MIPs (microtubule inner proteins), meaning they reside in the luminal space of microtubules [79–82]. Furthermore, luminal MAP6 can stabilize microtubule curvature [83], though it is unknown whether SAXO proteins also share this functionality. *Saxo2* is enriched in hair cell transcriptomic datasets from mice and zebrafish [53,55,84] but has not been functionally characterized.

Human *SAXO2* is located on 15q25.2 (Table 1), near several sensorineural deafness loci including *DFNA30* (gene unknown) [85], *DFNA68* (*HOMER*) [86,87], *DFNB48* (*CIB2*) [88,89], and *OTSC1* [90]. SHIELD reports that *SAXO2* maps to the *DFNA30* locus. The critical region for *DFNA30* lies between markers D15S151 and D15S130 (GRCh38:15:87053920-94168232) with a maximum LOD score for marker D15S1004

294 [85]. However, current genomic coordinates for *SAXO2* (GRCh38:15:82262818-
295 82284927) place it outside the *DFNA30* critical interval, 4.8 MB away from the closest
296 marker D15S151 and 11.5 MB away from D15S1004.

297 *3.3. Distinct localization patterns of Ankef1a, Odf3l2a, and Saxo2 in the kinocilium.*

298 To analyze the subcellular localization of Ankef1a, Odf3l2a, and Saxo2 in zebrafish
299 hair cells, we created stable transgenic fish expressing fluorescently-tagged versions of
300 these proteins under control of the hair cell-specific *myo6b* promoter (Figure 1F). Tagged
301 Ankef1a, Odf3l2a, and Saxo2 proteins all exhibit robust localization to the hair cell
302 kinocilium (Figure 1G).

303 We imaged the lateral cristae and neuromasts of live larvae at 5-6 dpf and encoded
304 differences in pixel intensity by applying the ImageJ "cool" lookup table to maximum z-
305 projections (Figure 2A1-D1, E-H). We also quantified fluorescence intensity in these
306 kinocilia and present the average fluorescence intensity distribution as a log2 mean grey
307 value over the most distal 32 µm (Figure 2A2-D2). For comparison, we also used the
308 *Tg(myo6b:yfp-Hsa.TUBA)idc16* line that expresses YFP-tagged alpha tubulin in hair cells,
309 marking both cytoplasmic and axonemal microtubules as well as a pool of unpolymerized
310 tubulin. As expected, YFP-TUBA is uniformly distributed along the length of the hair cell
311 kinocilium in the lateral cristae and neuromasts (Figure 2A1, A2, E). Ankef1a-GFP displays
312 a similarly uniform distribution from base to tip (Figure 2B1, B2, F). The distribution of
313 Odf3l2a-GFP is distinct from that of tubulin and Ankef1a, with Odf3l2a being more
314 restricted to the middle-proximal region of the kinocilium (Figure 2C1, C2, G). The
315 distribution of Saxo2-mKate2 is complementary to that of Odf3l2a, with enriched
316 localization to the distal region of the kinocilium and a depletion in the middle-proximal
317 zone (Figure 2D1, D2, H). Interestingly, we observe bent kinocilia in the lateral cristae of
318 Saxo2-mKate2 transgenics (Figure 2D1), a phenotype we do not observe in the other
319 transgenic lines or in non-transgenic siblings. Saxo2-GFP is also enriched in the distal
320 region (Figure S1A, B), but we do not observe kinocilial curvature in this line. Together,
321 these transgenes demonstrate that Ankef1a, Odf3l2a, and Saxo2 are cilia-associated
322 proteins and reveal distinct distribution patterns for each of these proteins in the kinocilia
323 of zebrafish hair cells.

324 *3.4. Ankef1a, Odf3l2a, and Saxo2 exhibit distinct localization patterns in the hair cell soma*
325 *that differ from cytoplasmic tubulin.*

326 To determine if Ankef1a, Odf3l2a, and Saxo2 also associate with cytoplasmic
327 tubulin, we compared the cytoplasmic distributions of these three transgenes to that of YFP-
328 TUBA in the soma of hair cells in the lateral crista (Figure 3). In the cytoplasm, the YFP-
329 TUBA signal is strongest in the apical subcuticular zone that lies just below the actin-rich
330 cuticular plate. Cytoplasmic microtubules are also evident (Figure 3A). Ankef1a-GFP is
331 largely excluded from the subcuticular zone and there is no obvious association with
332 cytoplasmic microtubules (Figure 3B). Instead, the Ankef1a-GFP signal is diffuse
333 throughout the perinuclear cytoplasm. In contrast to Ankef1a, Odf3l2a-GFP signal is
334 mostly absent from the cytoplasm, instead accumulating in the nucleus of some hair cells.
335 In neuromast hair cells, Ankef1a and Odf3l2a display similar localization patterns as in the
336 crista (Figure S2A, B). Lastly, Saxo2-mKate2 does not associate with cytoplasmic
337 microtubules and instead accumulates in the subcuticular zone beneath the apical cuticular

plate, marked here by GFP-tagged beta actin (Figure 3D-F). Saxo2-GFP displays a similar apical accumulation in the cell body (Figure 1G, S1A). In top-down views of neuromast hair cells, Saxo2-mKate2 accumulates in a ring-like structure surrounding the cuticular plate (Figure 3F). In summary, although Ankef1a, Odf3l2a, and Saxo2 all localize with tubulin in the kinocilium, none of these proteins share the same distribution pattern as YFP-TUBA in the hair cell soma, nor do their patterns overlap with one another.

3.5. Saxo2-mKate2 overexpression results in curved, truncated, and 'bulbed' kinocilia.

Next, we measured kinocilial height in the lateral crista to determine whether overexpression of Ankef1a, Odf3l2a, or Saxo2 influences kinocilial morphology. The average maximum heights of kinocilia in *YFP-TUBA*, *ankef1a-GFP*, and *odf3l2a-GFP* transgenics were statistically indistinguishable from their non-transgenic siblings (Figure 4A). In contrast to these single transgenic lines, we identified at least three independent lines for *saxo2-mKate2* which we categorize as "mild", "intermediate", and "severe" in terms of their kinocilial phenotypes (Figure 4B-E). A one-way ANOVA comparing the three *saxo2-mKate2* phenotypes and non-transgenic siblings reveals significant differences in kinocilial length ($F_{3,24} = 193.3$, $p < 2e\text{-}16$). Compared to non-transgenic siblings, maximum height is not affected in "mild" *saxo2-mKate2* transgenics, despite examples of curved kinocilia (Figure 4A-C; non-Tg, n = 8, mean = 35.4 µm; "mild", n = 8, mean = 35.3 µm; padj = 0.9858). However, both the "intermediate" and "severe" phenotypes have significantly shorter kinocilia compared to non-transgenic siblings (Figure 4A, D, E; "intermediate", n = 7 mean = 32.1 µm, padj < 0.0001; "severe", n = 5, mean = 26.1 µm, padj < 0.0001). Transgenics with the "intermediate" phenotype exhibit kinocilial curvature and bulbed tips marked by an accumulation of Saxo2-mKate2 (Figure 4D). Lastly, the "severe" Saxo2-mKate2 overexpression phenotype includes a further reduction in average maximum kinocilia height and increased prominence of bulbed tips (Figure 4E). The severe phenotype is also marked by a punctate accumulation of Saxo2-mKate2 in the cell bodies and along the kinocilia. Some of these puncta are bidirectionally mobile in the kinocilia (Video S1). Neuromasts from the severely affected larvae display a similar phenotype (Figure S3). Surprisingly, these "severe" *saxo2-mKate2* transgenics are viable and qualitatively do not exhibit obvious auditory or vestibular phenotypes as larvae or adults. The Saxo2-GFP line does not exhibit curved kinocilia nor a significant change in kinocilial height ($t = -1.8712$, $df = 5.5674$, p-value = 0.1143) (Figure S1C). In summary, transgenic expression of Ankef1a and Odf3l2a does not affect kinocilial height. This is also true of the Saxo2-mKate2 line with lower levels of expression though curved kinocilia are common. Transgenic lines with elevated Saxo2-mKate2 levels exhibit bulbed and truncated kinocilia.

3.6. Ankef1a, Odf3l2a, and tubulin distribution patterns are not influenced by Saxo2.

Given that Saxo2-mKate2 can alter kinocilial morphology, we next tested whether the presence of Saxo2-mKate2 influences the distributions of YFP-TUBA, Ankef1a-GFP, Odf3l2a-GFP, and Saxo2-GFP. We produced four combinations of double transgenic fish, each with Saxo2-mKate2 as a common factor. Co-expression of Saxo2-mKate2 with YFP-TUBA (Figure 5A1-5, Figure S4), Ankef1a-GFP (Figure 5B1-5), or Odf3l2a-GFP (Figure 5C1-5) did not alter the distribution patterns of either pair of proteins relative to single transgenic siblings. An example of the Saxo2-mKate2 "intermediate" phenotype is shown in panels B1, B3-5 while the "mild" phenotype is shown in the other examples. On the other hand, rather than simply overlap with one another, co-expression of Saxo2-mKate and

383 Saxo2-GFP reveals a form of competition for space between these two transgenic proteins
384 (Figure 5D1-5). Most obviously at the tips, either the mKate2 or GFP version of Saxo2 is
385 more abundant with Saxo2-mKate2 appearing to outcompete Saxo2-GFP at the tips of most
386 kinocilia. Taken together, these data suggest that Saxo2 does not positively or negatively
387 influence the distributions of tubulin, Ankef1a, or Odf3l2a in the kinocilium.

388 # 4. Discussion

389 *4.1. Utility of TU-tagging to identify hair cell transcripts.*

390 As with our previously published work [30], here we show that hair cell-enriched
391 transcripts can be identified by thiouracil tagging of newly synthesized RNA. GO analysis
392 confirms that hair cell transcripts are overrepresented in the TU-tagged samples. We also
393 identified all of the TU-enriched transcripts from our previously report, although some gene
394 identifiers from GRCz10 are no longer part of the current GRCz11 genome assembly
395 (*stereocilin-like* genes ENSDARG00000078845 and ENSDARG00000088059, *fam188b2*
396 ENSDARG00000069867, uncharacterized gene ENSDARG00000088304). Changes to the
397 experimental protocol greatly increased the number of significantly enriched genes in the
398 TU-tagged samples. However, in addition to an enrichment of genes related to hair cells
399 and cilia, this dataset is also enriched for genes involved in electron transport and ATP
400 synthesis, iron metabolism, and visual system development and function (Table S2). These
401 results confirm the signal-to-noise problem that seems inherit to TU-tagging in zebrafish.
402 Unless one's experiment requires time resolved differentiation between nascent and
403 preexisting pools of RNA, recent advances in single cell RNA sequencing have largely
404 rendered more error-prone techniques like TU-tagging obsolete.

405 *4.2. Determining the subcellular localization for putative kinocilial proteins.*

406 GFP-tagged proteins have long been valuable tools for live imaging of protein
407 localization [91,92]. This technique has proven particularly invaluable in the analysis of
408 protein localization and function in zebrafish hair cells [8,93–102]. GFP-tagging has also
409 been used extensively to assay for protein localization to microtubules and cilia [66,103–
410 106], including in hair cells [107]. MAP6 family members have also been studied in
411 cultured cells and in vitro using fluorescent protein tags, including MAP6-GFP
412 [83,108,109], and SAXO1- and SAXO2-GFP [76,77]. Importantly, the GFP-tag does not
413 seem to interfere with normal function or localization of cilia-associated proteins. MAP6-
414 GFP and endogenous MAP6 display similar enrichment in the proximal part of neuronal
415 axons [110], and GFP-tagged versions of the Eps15 homology domain proteins EHD1 and
416 EHD3 exhibit the same restricted localization to the proximal part of the primary cilium as
417 the endogenous protein [111]. Thus, GFP-tagging of cilial proteins is a powerful tool for
418 analyzing protein localization in live cells.

419 *4.3. Regionalization of the hair cell kinocilium.*

420 Primary cilia are compartmentalized along their proximal-distal axis into functional
421 domains marked by distinct protein compositions [112]. However, regionalization of the
422 hair cell kinocilium has received little attention. Here, we express tagged versions of hair
423 cell-enriched proteins Ankef1a, Odf3l2a, and Saxo2 in zebrafish to demonstrate their
424 localization to the kinocilium of hair cells. Live imaging of these transgenic proteins also
425 reveals their unique kinocilial localization patterns (Figure 6). Like YFP-tagged tubulin,

426 Ankef1a-GFP is uniformly distributed along the entire length of the kinocilium.
427 Interestingly, Odf3l2a and Saxo2 exhibit somewhat complementary localization patterns,
428 with Odf3l2a being restricted to the proximal-middle region and Saxo2 accumulating at the
429 kinocilial tips. Together, our study is the first to demonstrate cilial localization for these
430 proteins in hair cells and suggests the existence of regionalized protein localization domains
431 within the kinocilium. It remains to be tested whether these domains are important for
432 kinocilial structure and the sensory function of hair cells.

433 Based on our results, we propose that Ankef1a, Odf3l2a, and Saxo2 represent three
434 examples of proteins with distinct kinocilial localization or retention signals. Analogous to
435 how tubulin monomers line up in an orderly fashion, Ankef1a may contain a "queue-up"
436 motif that prevents accumulation once all available spots are filled, assuring an uniform
437 distribution of Ankef1a along the axoneme. Odf3l2a may encode a "stop" signal that
438 restricts localization to the middle-proximal compartment. Lastly, Saxo2 may contain a
439 "keep walking" signal that allows the protein to accumulate at the plus ends of the axonemal
440 microtubules. These putative localization or sorting motifs may interact with subunits of
441 the IFT machinery and / or with components of the transition zone or axoneme to produce
442 these three distinct kinocilial localization patterns. Our results lay the foundation for future
443 structure-function experiments to understand how these proteins are targeted to cilia and,
444 together with loss-of-function models, to characterize their functional domains.

445 *4.4. Saxo2 promotes formation of curved and truncated kinocilia.*

446 Kinocilial length and morphology are normal in our *ankef1a* and *odf3l2a*
447 transgenics. However, we find that Saxo2-mKate2 overexpression promotes the formation
448 of curved kinocilia. SAXO proteins are members of the microtubule associated protein 6
449 (MAP6) family that stabilize microtubules in axons, cilia, and flagella [75,76]. Recent work
450 shows that MAP6 and SAXO are microtubule inner proteins (MIPs) that can localize to the
451 intraluminal space of microtubules [79–81,83]. Full length MAP6 can bind to either the
452 outside or inside of microtubules, and intraluminal localization requires a N-terminal
453 cysteine-rich domain [83]. Luminal MAP6 can stabilize the formation of curved or helical
454 microtubules, a property that externally-bound MAP6 does not possess [83]. Saxo2 also
455 features the cysteine-rich N-terminal domain of the MAP6 family [77]. Given that only
456 luminal MAP6 induces microtubule curvature, it is likely that overexpressed Saxo2 also
457 uses its N-terminal domain to localize to the luminal space of the axonemal microtubules
458 in hair cells. Whether endogenous Saxo2 is a bona fide MIP in the kinocilium remains to
459 be determined. However, our TU-tagging dataset is also significantly enriched for other
460 known MIPs [113], including cilia and flagella associated proteins (Cfap20, 45, and 52),
461 EF-hand domain containing (Efhc) proteins 1 and 2, meiosis-specific nuclear structural 1
462 (Mns1), and Tektins 1-3 (Tables S2, S4). There are likely to be additional hair cell-enriched
463 MIPs and these data indicate a role for intraluminal microtubule associated proteins in our
464 senses of hearing and balance.

465 Saxo2 overexpression also promotes formation of bulbed kinocilia marked by an
466 accumulation of Saxo2 at the tip. This distal accumulation is not accompanied with a
467 concomitant redistribution of Ankef1a, Odf3l2a, or tubulin (Figure S4, Figure 5). This is
468 unlike the kinocilial bulb of bullfrog hair cells that labels strongly for beta tubulin [114].
469 Thus, it is likely that the "canonical" and Saxo2-induced bulbs form by different
470 mechanisms. We also report that Saxo2 overexpression promotes formation of truncated

471 kinocilia and that higher levels of Saxo2 expression are correlated with more severe
472 truncations (Figure 4). This correlation suggests that excess Saxo2 is commandeering the
473 intraflagellar transport (IFT) machinery, leading to Saxo2 accumulation at the tip, possibly
474 at the expense of other components required for normal growth of the kinocilium. However,
475 kinocilial length is unchanged in Saxo2 transgenics with more modest levels of expression
476 (Saxo2-mKate2 "mild" and Saxo2-GFP). Our results differ from those of Dacheux et al.
477 who reported that SAXO1 overexpression almost doubles the length of the primary cilium
478 in cultured RPE1 cells [76]. This discrepancy could be due to differences between the
479 SAXO proteins and / or cell types. We also note differences between the Saxo2-GFP and
480 Saxo2-mKate2 phenotypes. Although the tip-enriched distribution patterns are similar
481 between the two forms, we do not observe curvature or truncation of kinocilia in the Saxo2-
482 GFP line (Figure S1). However, as the Saxo2-mKate2 phenotype intensifies with higher
483 expression levels, we suspect that the comparatively lower levels of Saxo2-GFP expression
484 is the reason for the phenotypic discrepancy between the two tags. There is also reason to
485 believe that the mKate2 version of Saxo2 is trafficked more efficiently to the kinocilium –
486 qualitatively, we observe a greater accumulation of Saxo2-GFP in the subcuticular zone
487 relative to Saxo2-mKate2 and Saxo2-mKate2 tends to accumulate at the tips to the partial
488 exclusion of Saxo2-GFP when they are co-expressed (Figure 5). Although the formation of
489 bulbed and truncated kinocilia is likely an artifact of Saxo2 overexpression, the cellular
490 phenotype is nonetheless interesting for its lack of a behavioural correlate. The adult
491 viability and qualitatively normal behaviour of the severe Saxo2 phenotype suggests that a
492 partial disruption of kinocilial morphology is tolerated under laboratory settings. This
493 tolerance and possible genetic redundancy may account for why hair cell-enriched
494 kinocilial genes have not been identified in genetic screens based on specific auditory or
495 vestibular behavioural phenotypes [115].

496 *4.5. ANKEF1, ODF3L2, and SAXO2 as putative hearing loss genes.*

497 Although we and others have identified many genes that may contribute to form and
498 function of the hair cell kinocilium, we focused on *ankef1a*, *odf3l2a*, and *saxo2* for this
499 study based on preliminary reports of their genetic location in relation to mouse and human
500 deafness loci. Mouse *Ankef1* is within the coloboma (*Cm*) deletion locus, phenotypes of
501 which include planar polarity defects in the cochlear epithelium, supernumerary hair cells,
502 and hearing and balance defects [25,26]. Deletion of the Notch ligand gene *Jag1* is
503 responsible for most of these hearing-related phenotypes, but phenotypical differences
504 between *Cm* and *Jag1* heterozygotes leave open the possibility that other genes in the *Cm*
505 locus are contributing to the phenotype. Since ANKEF1 is a kinocilial protein and Notch
506 pathway mutants display polarity defects indicative of mispositioned kinocilia [116,117],
507 it is possible that the combined heterozygous loss of *Jag1* and *Ankef1* reveals a subtle role
508 for ANKEF1 in kinocilial development which would not be apparent otherwise. Since
509 ANKEF1 has protein-protein interaction Ankyrin repeats and calcium-sensing EF hand
510 domains, one may speculate that ANKEF1 mediates protein-protein interactions in the
511 kinocilium in response to changes in calcium concentrations.

512 A targeted knockout of *Odf3l2* in mice results in high frequency hearing loss and
513 vestibular deficits [67,118,119]. The cellular basis for these phenotypes is unclear as mouse
514 *Odf3l2* is not robustly expressed in either cochlear or vestibular hair cells [48,84,120].
515 However, *Odf3l2* expression is detected in outer pillar cells [120,121], suggesting a non-

516 hair cell basis for the mutant phenotype. Interestingly, the homologous *Odf3b* is strongly
517 expressed in mammalian hair cells, but the knockout mice do not exhibit auditory or
518 vestibular phenotypes [119]. Zebrafish *odf3l2a* is expressed in both inner ear and lateral
519 line hair cells (Figure 1C) [55,122] whereas *odf3b* is specifically expressed in ciliated cells
520 of the olfactory epithelia and pronephros [123]. Zebrafish have a second ortholog (*odf3l2b*)
521 whose expression is restricted to the testis [124]. Thus, vertebrate hair cells may utilize
522 different *ODF3* orthologs – *ODF3B* in mammals and *odf3l2a* in fish.

523 *Saxo2* transcripts are enriched in mouse cochlear and vestibular hair cells
524 [48,84,120,121] as well as the inner ear and lateral line hair cells of zebrafish (Figure 1D)
525 [55,122]. Enriched expression in the olfactory epithelia is also shared between mice and
526 fish [105]. However, unlike *Odf3l2*, there are no published loss-of-function animal models
527 for *Saxo2*. Human *SAXO2* (a.k.a. *FAM154B*) and *ODF3L2* were reported in SHIELD as
528 mapping to deafness loci *DFNA30* and *DFNB72*, respectively [27]. *DFNA30* is an
529 autosomal dominant form of nonsyndromic hearing loss for which the causative gene
530 remains unknown [85]. However, neither *SAXO2* or *ODF3L2* reside within any known
531 deafness loci based on our analysis of the genetic markers used to map these and other
532 nearby loci. Although it is still possible that ODF3L2 and SAXO2 contribute to auditory or
533 vestibular function, we propose they should be excluded as candidates for currently known
534 deafness loci.

535 *4.6. Benefits and limitations of this study.*

536 In contrast to the short primary cilium of most cell types, sensory hair cells, in
537 particular vestibular hair cells of the semicircular canals, possess very long kinocilia. This
538 study takes advantage of the long kinocilium in the cristae of larval zebrafish and the ability
539 to image tagged protein localization in live animals to understand more about the sub-
540 cellular and sub-cilial localization of these proteins. Benefits of live imaging of
541 fluorescently tagged proteins are i) avoiding morphological distortions caused by fixation
542 and processing, and ii) inconsistent antibody staining. Limitations include the possibility of
543 altered protein localization patterns caused by the fluorescent protein tag or from use of a
544 heterologous promoter to drive overexpression. However, the fact that all three proteins
545 tested here display unique kinocilial and cytoplasmic distributions patterns suggest that
546 these tagged proteins reflect their endogenous distribution patterns. An unexpected result
547 from this study is Odf3l2a-GFP localization to the nucleus. Immunostaining of the
548 endogenous protein is necessary to confirm this finding. If true, it presents the fascinating
549 possibility of a communication channel between the kinocilia and the nucleus.
550 Overexpression can also cause spurious phenotypes that may not be directly related to
551 protein function. For example, the bulbed and truncated kinocilia observed in the "severe"
552 Saxo2-mKate2 transgenic line may be an overexpression artifact caused by overloading the
553 IFT machinery with excess Saxo2. However, the curved kinocilia we observe is consistent
554 with previously reported function of MAP6-family proteins.

555 5. Conclusion

556 Here, we report hair cell-enriched expression of zebrafish *ankef1a*, *odf3l2a*, and
557 *saxo2,* and show that tagged versions of these protein exhibit distinct distribution patterns
558 within the kinocilium. Together, our results suggest that the hair cell kinocilium is
559 regionalized along its proximal-distal axis.

Supplementary Materials: Figures S1-4, Tables S1-4, Video S1.

Author Contributions: Conceptualization, T.E.; formal analysis, T.E.; investigation, T.E., W.P.B., K.W., S.E.B., and A.V.; data curation, T.E.; writing—original draft preparation, T.E.; writing—review and editing, T.E., A.V.; visualization, T.E., S.E.B., and A.V.; supervision, T.E.; project administration, T.E.; funding acquisition, T.E. All authors have read and agreed to the published version of the manuscript.

Funding: This work was supported by funding awarded to T.E. by the Collins Medical Trust, East Carolina University's Division of Research, Economic Development and Engagement (REDE), and The Natural Science and Engineering Research Council (NSERC) of Canada Discovery Grant RGPIN-2021-0316.

Institutional Review Board Statement: All procedures involving animals were performed in accordance with animal use protocols approved at Oregon Health & Science University (2065), East Carolina University (D352), and the University of New Brunswick (22007).

Data Availability Statement: Data and code will be provided by reasonable request from a qualified researcher.

Acknowledgments: This work was conducted at three institutions (OHSU, ECU, and UNB), intermittently over approximately eight years. A special thank you to Teresa Nicolson, in whose lab at OHSU this work was initiated. Thank you also to Amy Carlos and Robert Searles of the OHSU Massively Parallel Sequencing Shared Resource for performing the RNA sequencing experiments. Many thanks to the support staff in the Nicolson lab at OHSU and to the many students who have contributed to animal care at ECU and UNB. Thank you to Christine Erickson for making the hair cell diagrams.

Conflicts of Interest: The authors declare no conflict of interest.

584 ## 6. References

585 1. Bezares-Calderón, L.A.; Berger, J.; Jékely, G. Diversity of Cilia-Based
586 Mechanosensory Systems and Their Functions in Marine Animal Behaviour. *Philos*
587 *Trans R Soc Lond B Biol Sci* **2020**, *375*, 20190376, doi:10.1098/rstb.2019.0376.

588 2. Sharkova, M.; Chow, E.; Erickson, T.; Hocking, J.C. The Morphological and
589 Functional Diversity of Apical Microvilli. *J Anat* **2022**, doi:10.1111/joa.13781.

590 3. Jones, C.; Roper, V.C.; Foucher, I.; Qian, D.; Banizs, B.; Petit, C.; Yoder, B.K.;
591 Chen, P. Ciliary Proteins Link Basal Body Polarization to Planar Cell Polarity
592 Regulation. *Nat Genet* **2008**, *40*, 69–77, doi:10.1038/ng.2007.54.

593 4. Moon, K.-H.; Ma, J.-H.; Min, H.; Koo, H.; Kim, H.; Ko, H.W.; Bok, J. Dysregulation
594 of Sonic Hedgehog Signaling Causes Hearing Loss in Ciliopathy Mouse Models.
595 *Elife* **2020**, *9*, 1–63, doi:10.7554/eLife.56551.

596 5. Shi, H.; Wang, H.; Zhang, C.; Lu, Y.; Yao, J.; Chen, Z.; Xing, G.; Wei, Q.; Cao, X.
597 Mutations in OSBPL2 Cause Hearing Loss Associated with Primary Cilia Defects
598 via Sonic Hedgehog Signaling. *JCI Insight* **2022**, *7*, doi:10.1172/jci.insight.149626.

599 6. Baird, R.A. Comparative Transduction Mechanisms of Hair Cells in the Bullfrog
600 Utriculus. II. Sensitivity and Response Dynamics to Hair Bundle Displacement. *J*
601 *Neurophysiol* **1994**, *71*, 685–705, doi:10.1152/jn.1994.71.2.685.

602 7. Spoon, C.; Grant, W. Biomechanics of Hair Cell Kinocilia: Experimental
603 Measurement of Kinocilium Shaft Stiffness and Base Rotational Stiffness with
604 Euler–Bernoulli and Timoshenko Beam Analysis. *Journal of Experimental Biology*
605 **2011**, *214*, 862–870, doi:10.1242/jeb.051151.

606 8. Kindt, K.S.; Finch, G.; Nicolson, T. Kinocilia Mediate Mechanosensitivity in
607 Developing Zebrafish Hair Cells. *Dev Cell* **2012**, *23*, 329–341,
608 doi:10.1016/j.devcel.2012.05.022.

609 9. Stooke-Vaughan, G.A.; Huang, P.; Hammond, K.L.; Schier, A.F.; Whitfield, T.T.
610 The Role of Hair Cells, Cilia and Ciliary Motility in Otolith Formation in the
611 Zebrafish Otic Vesicle. *Development* **2012**, *139*, 1777–1787,
612 doi:10.1242/dev.079947.

613 10. Sobkowicz, H.M.; Slapnick, S.M.; August, B.K. The Kinocilium of Auditory Hair
614 Cells and Evidence for Its Morphogenetic Role during the Regeneration of
615 Stereocilia and Cuticular Plates. *J Neurocytol* **1995**, *24*, 633–653,
616 doi:10.1007/BF01179815.

617 11. Flock, A.; Duvall, A.J. The Ultrastructure of the Kinocilium of the Sensory Cells in
618 the Inner Ear and Lateral Line Organs. *Journal of Cell Biology* **1965**, *25*, 1–8,
619 doi:10.1083/jcb.25.1.1.

620 12. Kikuchi, T.; Takasaka, T.; Tonosaki, A.; Watanabe, H. Fine Structure of Guinea Pig
621 Vestibular Kinocilium. *Acta Otolaryngol* **1989**, *108*, 26–30,
622 doi:10.3109/00016488909107388.

623 13. Burton, P.R. Ultrastructural Studies of Microtubules and Microtubule Organizing
624 Centers of the Vertebrate Olfactory Neuron. *Microsc Res Tech* **1992**, *23*, 142–156,
625 doi:10.1002/jemt.1070230205.

626 14. Rüsch, A.; Thurm, U. Passive and Active Deflections of Ampullary Kinocilia
627 Correlated with Changes in Transepithelial Voltage. *ORL* **1986**, *48*, 76–80,
628 doi:10.1159/000275849.

629 15. Rüsch, A.; Thurm, U. Spontaneous and Electrically Induced Movements of
630 Ampullary Kinocilia and Stereovilli. *Hear Res* **1990**, *48*, 247–263,
631 doi:10.1016/0378-5955(90)90065-W.

632 16. Alstrom, C.H.; Hallgren, B.; Nilsson, L.; Asander, H. Retinal Degeneration
633 Combined with Obesity, Diabetes Mellitus and Neurogenous Deafness: A Specific
634 Syndrome (Not Hitherto Described) Distinct from the Laurence-Moon-Bardet-Biedl
635 Syndrome: A Clinical, Endocrinological and Genetic Examination Based on a Large
636 Pedigree. *Acta Psychiatr Neurol Scand Suppl* **1959**, *129*, 1–35.

637 17. Ross, A.J.; May-Simera, H.; Eichers, E.R.; Kai, M.; Hill, J.; Jagger, D.J.; Leitch,
638 C.C.; Chapple, J.P.; Munro, P.M.; Fisher, S.; et al. Disruption of Bardet-Biedl
639 Syndrome Ciliary Proteins Perturbs Planar Cell Polarity in Vertebrates. *Nature*
640 *Genetics 2005 37:10* **2005**, *37*, 1135–1140, doi:10.1038/ng1644.

641 18. Jagger, D.; Collin, G.; Kelly, J.; Towers, E.; Nevill, G.; Longo-Guess, C.; Benson,
642 J.; Halsey, K.; Dolan, D.; Marshall, J.; et al. Alström Syndrome Protein ALMS1
643 Localizes to Basal Bodies of Cochlear Hair Cells and Regulates Cilium-Dependent
644 Planar Cell Polarity. *Hum Mol Genet* **2011**, *20*, 466–481, doi:10.1093/hmg/ddq493.

645 19. Modamio-Høybjør, S.; Mencía, Á.; Goodyear, R.; del Castillo, I.; Richardson, G.;
646 Moreno, F.; Moreno-Pelayo, M.Á. A Mutation in CCDC50, a Gene Encoding an
647 Effector of Epidermal Growth Factor-Mediated Cell Signaling, Causes Progressive
648 Hearing Loss. *Am J Hum Genet* **2007**, *80*, 1076–1089, doi:10.1086/518311.

649 20. Cui, L.; Zheng, J.; Zhao, Q.; Chen, J.-R.; Liu, H.; Peng, G.; Wu, Y.; Chen, C.; He,
650 Q.; Shi, H.; et al. Mutations of MAP1B Encoding a Microtubule-Associated
651 Phosphoprotein Cause Sensorineural Hearing Loss. *JCI Insight* **2020**, *5*,
652 doi:10.1172/jci.insight.136046.

653 21. Grati, M.; Chakchouk, I.; Ma, Q.; Bensaid, M.; Desmidt, A.; Turki, N.; Yan, D.;
654 Baanannou, A.; Mittal, R.; Driss, N.; et al. A Missense Mutation in DCDC2 Causes
655 Human Recessive Deafness DFNB66, Likely by Interfering with Sensory Hair Cell
656 and Supporting Cell Cilia Length Regulation. *Hum Mol Genet* **2015**, *24*, 2482–2491,
657 doi:10.1093/hmg/ddv009.

658 22. Bork, J.M.; Peters, L.M.; Riazuddin, S.; Ahmed, Z.M.; Li, X.C.; Griffith, A.J.;
659 Wilcox, E.R.; Friedman, T.B.; Morell, R.J.; Griffith, A.J.; et al. Usher Syndrome 1D
660 and Nonsyndromic Autosomal Recessive Deafness DFNB12 Are Caused by Allelic
661 Mutations of the Novel Cadherin-like Gene CDH23. *Am J Hum Genet* **2001**, *68*, 26–
662 37, doi:10.1086/316954.

663 23. Ahmed, Z.M. PCDH15 Is Expressed in the Neurosensory Epithelium of the Eye and
664 Ear and Mutant Alleles Are Responsible for Both USH1F and DFNB23. *Hum Mol*
665 *Genet* **2003**, *12*, 3215–3223, doi:10.1093/hmg/ddg358.

666 24. Pickett, S.B.; Raible, D.W. Water Waves to Sound Waves: Using Zebrafish to
667 Explore Hair Cell Biology. *Journal of the Association for Research in*
668 *Otolaryngology* **2019**, *20*, 1–19, doi:10.1007/s10162-018-00711-1.

669 25. Gunn, R.K.; Keenan, M.-E.; Brown, R.E. Analysis of Sensory, Motor and Cognitive
670 Functions of the Coloboma (C3Sn.Cg-Cm/J) Mutant Mouse. *Genes Brain Behav*
671 **2011**, *10*, 579–588, doi:10.1111/j.1601-183X.2011.00697.x.

672 26. Kiernan, A.E.; Ahituv, N.; Fuchs, H.; Balling, R.; Avraham, K.B.; Steel, K.P.; Hrabé
673 de Angelis, M. The Notch Ligand Jagged1 Is Required for Inner Ear Sensory
674 Development. *Proc Natl Acad Sci U S A* **2001**, *98*, 3873–3878,
675 doi:10.1073/pnas.071496998.

676 27. Shen, J.; Scheffer, D.I.; Kwan, K.Y.; Corey, D.P. SHIELD: An Integrative Gene
677 Expression Database for Inner Ear Research. *Database (Oxford)* **2015**, *2015*,
678 bav071, doi:10.1093/database/bav071.

679 28. Westerfield, M. *The Zebrafish Book. A Guide for the Laboratory Use of Zebrafish*
680 *(Danio Rerio).*; 4th ed.; University of Oregon: Eugene OR, 2000;

681 29. Ohta, S.; Ji, Y.R.; Martin, D.; Wu, D.K. Emx2 Regulates Hair Cell Rearrangement
682 but Not Positional Identity within Neuromasts. *Elife* **2020**, *9*, 1–69,
683 doi:10.7554/eLife.60432.

684 30. Erickson, T.; Nicolson, T. Identification of Sensory Hair-Cell Transcripts by
685 Thiouracil-Tagging in Zebrafish. *BMC Genomics* **2015**, *16*, 842,
686 doi:10.1186/s12864-015-2072-5.

687 31. Kwan, K.M.; Fujimoto, E.; Grabher, C.; Mangum, B.D.; Hardy, M.E.; Campbell,
688 D.S.; Parant, J.M.; Yost, H.J.; Kanki, J.P.; Chien, C.-B. The Tol2kit: A Multisite
689 Gateway-Based Construction Kit for Tol2 Transposon Transgenesis Constructs.
690 *Developmental Dynamics* **2007**, *236*, 3088–3099, doi:10.1002/dvdy.21343.

691 32. Afgan, E.; Baker, D.; van den Beek, M.; Blankenberg, D.; Bouvier, D.; Čech, M.;
692 Chilton, J.; Clements, D.; Coraor, N.; Eberhard, C.; et al. The Galaxy Platform for
693 Accessible, Reproducible and Collaborative Biomedical Analyses: 2016 Update.
694 *Nucleic Acids Res* **2016**, *44*, W3–W10, doi:10.1093/nar/gkw343.

695 33. Thomas, P.D.; Ebert, D.; Muruganujan, A.; Mushayahama, T.; Albou, L.-P.; Mi, H.
696 PANTHER: Making Genome-Scale Phylogenetics Accessible to All. *Protein Sci*
697 **2022**, *31*, 8–22, doi:10.1002/pro.4218.

698 34. Mi, H.; Muruganujan, A.; Huang, X.; Ebert, D.; Mills, C.; Guo, X.; Thomas, P.D.
699 Protocol Update for Large-Scale Genome and Gene Function Analysis with the
700 PANTHER Classification System (v.14.0). *Nature Protocols 2019 14:3* **2019**, *14*,
701 703–721, doi:10.1038/s41596-019-0128-8.

702 35. van Camp, G.; Smith, R.J.H. Hereditary Hearing Loss Homepage Available online:
703 https://hereditaryhearingloss.org (accessed on 29 December 2022).

704 36. Cunningham, F.; Allen, J.E.; Allen, J.; Alvarez-Jarreta, J.; Amode, M.R.; Armean,
705 I.M.; Austine-Orimoloye, O.; Azov, A.G.; Barnes, I.; Bennett, R.; et al. Ensembl
706 2022. *Nucleic Acids Res* **2022**, *50*, D988–D995, doi:10.1093/NAR/GKAB1049.

707 37. Schindelin, J.; Arganda-Carreras, I.; Frise, E.; Kaynig, V.; Longair, M.; Pietzsch, T.;
708 Preibisch, S.; Rueden, C.; Saalfeld, S.; Schmid, B.; et al. Fiji: An Open-Source
709 Platform for Biological-Image Analysis. *Nat Methods* **2012**, *9*, 676–682,
710 doi:10.1038/nmeth.2019.

711 38. Schneider, C.A.; Rasband, W.S.; Eliceiri, K.W. NIH Image to ImageJ: 25 Years of
712 Image Analysis. *Nat Methods* **2012**, *9*, 671–675, doi:10.1038/nmeth.2089.

713 39. Arshadi, C.; Günther, U.; Eddison, M.; Harrington, K.I.S.; Ferreira, T.A. SNT: A
714 Unifying Toolbox for Quantification of Neuronal Anatomy. *Nature Methods 2021*
715 *18:4* **2021**, *18*, 374–377, doi:10.1038/s41592-021-01105-7.

716 40. RStudio Team RStudio: Integrated Development Environment for R 2022.

717 41. R Core Team R: A Language and Environment for Statistical Computing 2022.

718 42. Wickham, H. Ggplot2. *Wiley Interdiscip Rev Comput Stat* **2011**, *3*, 180–185,
719 doi:10.1002/wics.147.

720 43. Miller, M.R.; Robinson, K.J.; Cleary, M.D.; Doe, C.Q. TU-Tagging: Cell Type-
721 Specific RNA Isolation from Intact Complex Tissues. *Nat Methods* **2009**, *6*, 439–
722 441, doi:10.1038/nmeth.1329.

723 44. Daniel, J.G.; Panizzi, J.R. Spatiotemporal Expression Profile of Embryonic and
724 Adult Ankyrin Repeat and EF-Hand Domain Containing Protein 1-Encoding Genes
725 Ankef1a and Ankef1b in Zebrafish. *Gene Expression Patterns* **2019**, *34*, 119069,
726 doi:10.1016/j.gep.2019.119069.

727 45. Scott, E.K.; Mason, L.; Arrenberg, A.B.; Ziv, L.; Gosse, N.J.; Xiao, T.; Chi, N.C.;
728 Asakawa, K.; Kawakami, K.; Baier, H. Targeting Neural Circuitry in Zebrafish
729 Using GAL4 Enhancer Trapping. *Nature Methods 2007 4:4* **2007**, *4*, 323–326,
730 doi:10.1038/nmeth1033.

731 46. Chung, H.A.; Yamamoto, T.S.; Ueno, N. ANR5, an FGF Target Gene Product,
732 Regulates Gastrulation in Xenopus. *Current Biology* **2007**, *17*, 932–939,
733 doi:10.1016/j.cub.2007.04.034.

734 47. di Domenico, F. The Role of Ankef1 in Male Fertility, Icahn School of Medicine at
735 Mount Sinai: New York, 2021.

736 48. Jan, T.A.; Eltawil, Y.; Ling, A.H.; Chen, L.; Ellwanger, D.C.; Heller, S.; Cheng,
737 A.G. Spatiotemporal Dynamics of Inner Ear Sensory and Non-Sensory Cells
738 Revealed by Single-Cell Transcriptomics. *Cell Rep* **2021**, *36*, 109358,
739 doi:10.1016/j.celrep.2021.109358.

740 49. Hoh, R.A.; Stowe, T.R.; Turk, E.; Stearns, T. Transcriptional Program of Ciliated
741 Epithelial Cells Reveals New Cilium and Centrosome Components and Links to
742 Human Disease. *PLoS One* **2012**, *7*, e52166, doi:10.1371/journal.pone.0052166.

743 50. Baker, M.A.; Hetherington, L.; Reeves, G.M.; Aitken, R.J. The Mouse Sperm
744 Proteome Characterizedvia IPG Strip Prefractionation and LC-MS/MS
745 Identification. *Proteomics* **2008**, *8*, 1720–1730, doi:10.1002/pmic.200701020.

746 51. Baker, M.A.; Hetherington, L.; Reeves, G.; Müller, J.; Aitken, R.J. The Rat Sperm
747 Proteome Characterized ***via*** IPG Strip Prefractionation and LC-MS/MS
748 Identification. *Proteomics* **2008**, *8*, 2312–2321, doi:10.1002/pmic.200700876.

749 52. Blackburn, K.; Bustamante-Marin, X.; Yin, W.; Goshe, M.B.; Ostrowski, L.E.
750 Quantitative Proteomic Analysis of Human Airway Cilia Identifies Previously
751 Uncharacterized Proteins of High Abundance. *J Proteome Res* **2017**, *16*, 1579–1592,
752 doi:10.1021/acs.jproteome.6b00972.

753 53. Elkon, R.; Milon, B.; Morrison, L.; Shah, M.; Vijayakumar, S.; Racherla, M.; Leitch,
754 C.C.; Silipino, L.; Hadi, S.; Weiss-Gayet, M.; et al. RFX Transcription Factors Are
755 Essential for Hearing in Mice. *Nat Commun* **2015**, *6*, 8549,
756 doi:10.1038/ncomms9549.

757 54. Lush, M.E.; Diaz, D.C.; Koenecke, N.; Baek, S.; Boldt, H.; St Peter, M.K.; Gaitan-
758 Escudero, T.; Romero-Carvajal, A.; Busch-Nentwich, E.M.; Perera, A.G.; et al.
759 ScRNA-Seq Reveals Distinct Stem Cell Populations That Drive Hair Cell
760 Regeneration after Loss of Fgf and Notch Signaling. *Elife* **2019**, *8*,
761 doi:10.7554/eLife.44431.

762 55. Barta, C.L.; Liu, H.; Chen, L.; Giffen, K.P.; Li, Y.; Kramer, K.L.; Beisel, K.W.; He,
763 D.Z. RNA-Seq Transcriptomic Analysis of Adult Zebrafish Inner Ear Hair Cells. *Sci*
764 *Data* **2018**, *5*, 180005, doi:10.1038/sdata.2018.5.

765 56. Hess, E.J.; Collins, K.A.; Copeland, N.G.; Jenkins, N.A.; Wilson, M.C. Deletion
766 Map of the Coloboma (Cm) Locus on Mouse Chromosome 2. *Genomics* **1994**, *21*,
767 257–261, doi:10.1006/geno.1994.1254.

768 57. Blake, J.A.; Baldarelli, R.; Kadin, J.A.; Richardson, J.E.; Smith, C.L.; Bult, C.J.;
769 Anagnostopoulos, A. v; Beal, J.S.; Bello, S.M.; Blodgett, O.; et al. Mouse Genome
770 Database (MGD): Knowledgebase for Mouse–Human Comparative Biology.
771 *Nucleic Acids Res* **2021**, *49*, D981–D987, doi:10.1093/nar/gkaa1083.

772 58. Hess, E.; Jinnah, H.; Kozak, C.; Wilson, M. Spontaneous Locomotor Hyperactivity
773 in a Mouse Mutant with a Deletion Including the Snap Gene on Chromosome 2. *The*
774 *Journal of Neuroscience* **1992**, *12*, 2865–2874, doi:10.1523/JNEUROSCI.12-07-
775 02865.1992.

776 59. Egydio de Carvalho, C.; Tanaka, H.; Iguchi, N.; Ventelä, S.; Nojima, H.; Nishimune,
777 Y. Molecular Cloning and Characterization of a Complementary DNA Encoding
778 Sperm Tail Protein SHIPPO 11. *Biol Reprod* **2002**, *66*, 785–795,
779 doi:10.1095/biolreprod66.3.785.

780 60. Dorus, S.; Busby, S.A.; Gerike, U.; Shabanowitz, J.; Hunt, D.F.; Karr, T.L. Genomic
781 and Functional Evolution of the Drosophila Melanogaster Sperm Proteome. *Nat*
782 *Genet* **2006**, *38*, 1440–1445, doi:10.1038/ng1915.

783 61. Konno, A.; Padma, P.; Ushimaru, Y.; Inaba, K. Multidimensional Analysis of
784 Uncharacterized Sperm Proteins in *Ciona Intestinalis* : EST-Based Analysis and

785 Functional Immunoscreening of Testis-Expressed Genes. *Zoolog Sci* **2010**, *27*, 204–
786 215, doi:10.2108/zsj.27.204.

787 62. Konno, A.; Shiba, K.; Cai, C.; Inaba, K. Branchial Cilia and Sperm Flagella Recruit
788 Distinct Axonemal Components. *PLoS One* **2015**, *10*, e0126005,
789 doi:10.1371/journal.pone.0126005.

790 63. White-Cooper, H. Studying How Flies Make Sperm—Investigating Gene Function
791 in Drosophila Testes. *Mol Cell Endocrinol* **2009**, *306*, 66–74,
792 doi:10.1016/j.mce.2008.11.026.

793 64. Bastin, B.R. Evolution of Tektin and ODF3 Family Genes and the Role of Gene
794 Duplication in the Specialization of Motile Ciliary Structures in the Polychaete
795 Platynereis Dumerilii, Iowa State University, 2018.

796 65. Lauwaet, T.; Smith, A.J.; Reiner, D.S.; Romijn, E.P.; Wong, C.C.L.; Davids, B.J.;
797 Shah, S.A.; Yates, J.R.; Gillin, F.D. Mining the Giardia Genome and Proteome for
798 Conserved and Unique Basal Body Proteins. *Int J Parasitol* **2011**, *41*, 1079–1092,
799 doi:10.1016/j.ijpara.2011.06.001.

800 66. Fong, K.; Leung, J.W.; Li, Y.; Wang, W.; Feng, L.; Ma, W.; Liu, D.; Songyang, Z.;
801 Chen, J. MTR120/KIAA1383, a Novel Microtubule-Associated Protein, Promotes
802 Microtubule Stability and Ensures Cytokinesis. *J Cell Sci* **2013**, *126*, 825–837,
803 doi:10.1242/jcs.116137.

804 67. Bowl, M.R.; Simon, M.M.; Ingham, N.J.; Greenaway, S.; Santos, L.; Cater, H.;
805 Taylor, S.; Mason, J.; Kurbatova, N.; Pearson, S.; et al. A Large Scale Hearing Loss
806 Screen Reveals an Extensive Unexplored Genetic Landscape for Auditory
807 Dysfunction. *Nat Commun* **2017**, *8*, 886, doi:10.1038/s41467-017-00595-4.

808 68. Rehman, A.U.; Gul, K.; Morell, R.J.; Lee, K.; Ahmed, Z.M.; Riazuddin, S.; Ali,
809 R.A.; Shahzad, M.; Jaleel, A.; Andrade, P.B.; et al. Mutations of GIPC3 Cause
810 Nonsyndromic Hearing Loss DFNB72 but Not DFNB81 That Also Maps to
811 Chromosome 19p. *Hum Genet* **2011**, *130*, 759–765, doi:10.1007/s00439-011-1018-
812 5.

813 69. Charizopoulou, N.; Lelli, A.; Schraders, M.; Ray, K.; Hildebrand, M.S.; Ramesh, A.;
814 Srisailapathy, C.R.S.; Oostrik, J.; Admiraal, R.J.C.; Neely, H.R.; et al. Gipc3
815 Mutations Associated with Audiogenic Seizures and Sensorineural Hearing Loss in
816 Mouse and Human. *Nat Commun* **2011**, *2*, 201, doi:10.1038/ncomms1200.

817 70. Santos-Cortez, R.L.P.; Faridi, R.; Rehman, A.U.; Lee, K.; Ansar, M.; Wang, X.;
818 Morell, R.J.; Isaacson, R.; Belyantseva, I.A.; Dai, H.; et al. Autosomal-Recessive
819 Hearing Impairment Due to Rare Missense Variants within S1PR2. *Am J Hum Genet*
820 **2016**, *98*, 331–338, doi:10.1016/j.ajhg.2015.12.004.

821 71. Jenkinson, E.M.; Rehman, A.U.; Walsh, T.; Clayton-Smith, J.; Lee, K.; Morell, R.J.;
822 Drummond, M.C.; Khan, S.N.; Naeem, M.A.; Rauf, B.; et al. Perrault Syndrome Is
823 Caused by Recessive Mutations in CLPP, Encoding a Mitochondrial ATP-
824 Dependent Chambered Protease. *Am J Hum Genet* **2013**, *92*, 605–613,
825 doi:10.1016/j.ajhg.2013.02.013.

72. Bönsch, D.; Schmidt, C.M.; Scheer, P.; Bohlender, J.; Neumann, C.; am Zehnhoff-Dinnesen, A.; Deufel, T. Ein Neuer Genort Für Eine Autosomal Dominante, Nichtsyndromale Hörstörung (DFNA57) Kartiert Auf Chromosom 19p13.2 Und Überlappt Mit DFNB15. *HNO* **2008**, *56*, 177–182, doi:10.1007/s00106-007-1633-6.

73. Ain, Q.; Nazli, S.; Riazuddin, S.; Jaleel, A.; Riazuddin, S.A.; Zafar, A.U.; Khan, S.N.; Husnain, T.; Griffith, A.J.; Ahmed, Z.M.; et al. The Autosomal Recessive Nonsyndromic Deafness Locus DFNB72 Is Located on Chromosome 19p13.3. *Hum Genet* **2007**, *122*, 445–450, doi:10.1007/s00439-007-0418-z.

74. Cuveillier, C.; Boulan, B.; Ravanello, C.; Denarier, E.; Deloulme, J.-C.; Gory-Fauré, S.; Delphin, C.; Bosc, C.; Arnal, I.; Andrieux, A. Beyond Neuronal Microtubule Stabilization: MAP6 and CRMPS, Two Converging Stories. *Front Mol Neurosci* **2021**, *14*, 82, doi:10.3389/fnmol.2021.665693.

75. Dacheux, D.; Landrein, N.; Thonnus, M.; Gilbert, G.; Sahin, A.; Wodrich, H.; Robinson, D.R.; Bonhivers, M. A MAP6-Related Protein Is Present in Protozoa and Is Involved in Flagellum Motility. *PLoS One* **2012**, *7*, e31344, doi:10.1371/journal.pone.0031344.

76. Dacheux, D.; Roger, B.; Bosc, C.; Landrein, N.; Roche, E.; Chansel, L.; Trian, T.; Andrieux, A.; Papaxanthos-Roche, A.; Marthan, R.; et al. Human FAM154A (SAXO1) Is a Microtubule-Stabilizing Protein Specific to Cilia and Related Structures. *J Cell Sci* **2015**, *128*, 1294–1307, doi:10.1242/jcs.155143.

77. Onyeneho, I.A. Microtubule Stability Mediated by New Mammalian STOP Family Members, Stanford University, 2014.

78. Kim, K.; Gibboney, S.; Razy-Krajka, F.; Lowe, E.K.; Wang, W.; Stolfi, A. Regulation of Neurogenesis by FGF Signaling and Neurogenin in the Invertebrate Chordate Ciona. *Front Cell Dev Biol* **2020**, *8*, 477, doi:10.3389/fcell.2020.00477.

79. Leung, M.R.; Roelofs, M.C.; Chiozzi, R.Z.; Hevler, J.F.; Heck, A.J.R.; Zeev-Ben-Mordehai, T. Unraveling the Intricate Microtubule Inner Protein Networks That Reinforce Mammalian Sperm Flagella. *bioRxiv* **2022**, 2022.09.29.510157, doi:10.1101/2022.09.29.510157.

80. Gui, M.; Wang, X.; Dutcher, S.K.; Brown, A.; Zhang, R. Ciliary Central Apparatus Structure Reveals Mechanisms of Microtubule Patterning. *Nat Struct Mol Biol* **2022**, *29*, 483–492, doi:10.1038/s41594-022-00770-2.

81. Gui, M.; Croft, J.T.; Zabeo, D.; Acharya, V.; Kollman, J.M.; Burgoyne, T.; Höög, J.L.; Brown, A. SPACA9 Is a Lumenal Protein of Human Ciliary Singlet and Doublet Microtubules. *Proc Natl Acad Sci U S A* **2022**, *119*, e2207605119, doi:10.1073/pnas.2207605119.

82. Ichikawa, M.; Bui, K.H. Microtubule Inner Proteins: A Meshwork of Luminal Proteins Stabilizing the Doublet Microtubule. *BioEssays* **2018**, *40*, 1700209, doi:10.1002/bies.201700209.

83. Cuveillier, C.; Delaroche, J.; Seggio, M.; Gory-Fauré, S.; Bosc, C.; Denarier, E.; Bacia, M.; Schoehn, G.; Mohrbach, H.; Kulić, I.; et al. MAP6 Is an Intraluminal

867 Protein That Induces Neuronal Microtubules to Coil. *Sci Adv* **2020**, *6*,
868 doi:10.1126/sciadv.aaz4344.

869 84. Wilkerson, B.A.; Zebroski, H.L.; Finkbeiner, C.R.; Chitsazan, A.D.; Beach, K.E.;
870 Sen, N.; Zhang, R.C.; Bermingham-McDonogh, O. Novel Cell Types and
871 Developmental Lineages Revealed by Single-Cell RNA-Seq Analysis of the Mouse
872 Crista Ampullaris. *Elife* **2021**, *10*, doi:10.7554/eLife.60108.

873 85. Mangino, M.; Flex, E.; Capon, F.; Sangiuolo, F.; Carraro, E.; Gualandi, F.; Mazzoli,
874 M.; Martini, A.; Novelli, G.; Dallapiccola, B. Mapping of a New Autosomal
875 Dominant Nonsyndromic Hearing Loss Locus (DFNA30) to Chromosome 15q25-
876 26. *European Journal of Human Genetics* **2001**, *9*, 667–671,
877 doi:10.1038/sj.ejhg.5200707.

878 86. Azaiez, H.; Decker, A.R.; Booth, K.T.; Simpson, A.C.; Shearer, A.E.; Huygen,
879 P.L.M.; Bu, F.; Hildebrand, M.S.; Ranum, P.T.; Shibata, S.B.; et al. HOMER2, a
880 Stereociliary Scaffolding Protein, Is Essential for Normal Hearing in Humans and
881 Mice. *PLoS Genet* **2015**, *11*, e1005137, doi:10.1371/journal.pgen.1005137.

882 87. Lu, X.; Wang, Q.; Gu, H.; Zhang, X.; Qi, Y.; Liu, Y. Whole Exome Sequencing
883 Identified a Second Pathogenic Variant in HOMER2 for Autosomal Dominant Non-
884 Syndromic Deafness. *Clin Genet* **2018**, *94*, 419–428, doi:10.1111/cge.13422.

885 88. Ahmad, J.; Khan, S.N.; Khan, S.Y.; Ramzan, K.; Riazuddin, S.; Ahmed, Z.M.;
886 Wilcox, E.R.; Friedman, T.B.; Riazuddin, S. DFNB48, a New Nonsyndromic
887 Recessive Deafness Locus, Maps to Chromosome 15q23-Q25.1. *Hum Genet* **2005**,
888 *116*, 407–412, doi:10.1007/s00439-004-1247-y.

889 89. Riazuddin, S.; Belyantseva, I.A.; Giese, A.P.J.; Lee, K.; Indzhykulian, A.A.;
890 Nandamuri, S.P.; Yousaf, R.; Sinha, G.P.; Lee, S.; Terrell, D.; et al. Alterations of
891 the CIB2 Calcium- and Integrin-Binding Protein Cause Usher Syndrome Type 1J
892 and Nonsyndromic Deafness DFNB48. *Nat Genet* **2012**, *44*, 1265–1271,
893 doi:10.1038/ng.2426.

894 90. Tomek, M.S.; Brown, M.R.; Mani, S.R.; Ramesh, A.; Srisailapathy, C.R.; Coucke,
895 P.; Zbar, R.I.; Bell, A.M.; McGuirt, W.T.; Fukushima, K.; et al. Localization of a
896 Gene for Otosclerosis to Chromosome 15q25-Q26. *Hum Mol Genet* **1998**, *7*, 285–
897 290, doi:10.1093/hmg/7.2.285.

898 91. Wang, S.; Hazelrigg, T. Implications for Bcd MRNA Localization from Spatial
899 Distribution of Exu Protein in Drosophila Oogenesis. *Nature* **1994**, *369*, 400–403,
900 doi:10.1038/369400a0.

901 92. Gerdes, H.-H.; Kaether, C. Green Fluorescent Protein: Applications in Cell Biology.
902 *FEBS Lett* **1996**, *389*, 44–47, doi:10.1016/0014-5793(96)00586-8.

903 93. Sheets, L.; He, X.J.; Olt, J.; Schreck, M.; Petralia, R.S.; Wang, Y.-X.; Zhang, Q.;
904 Beirl, A.; Nicolson, T.; Marcotti, W.; et al. Enlargement of Ribbons in Zebrafish
905 Hair Cells Increases Calcium Currents But Disrupts Afferent Spontaneous Activity
906 and Timing of Stimulus Onset. *The Journal of Neuroscience* **2017**, *37*, 6299–6313,
907 doi:10.1523/JNEUROSCI.2878-16.2017.

908 94. Maeda, R.; Pacentine, I.V.; Erickson, T.; Nicolson, T. Functional Analysis of the
909 Transmembrane and Cytoplasmic Domains of Pcdh15a in Zebrafish Hair Cells. *J*
910 *Neurosci* **2017**, *37*, 3231–3245, doi:10.1523/JNEUROSCI.2216-16.2017.

911 95. Erickson, T.; Pacentine, I.V.; Venuto, A.; Clemens, R.; Nicolson, T. The Lhfpl5
912 Ohnologs Lhfpl5a and Lhfpl5b Are Required for Mechanotransduction in Distinct
913 Populations of Sensory Hair Cells in Zebrafish. *Front Mol Neurosci* **2020**, *12*, 320,
914 doi:10.3389/fnmol.2019.00320.

915 96. Erickson, T.; Morgan, C.P.; Olt, J.; Hardy, K.; Busch-Nentwich, E.; Maeda, R.;
916 Clemens, R.; Krey, J.F.; Nechiporuk, A.; Barr-Gillespie, P.G.; et al. Integration of
917 Tmc1/2 into the Mechanotransduction Complex in Zebrafish Hair Cells Is Regulated
918 by Transmembrane O-Methyltransferase (Tomt). *Elife* **2017**, *6*,
919 doi:10.7554/eLife.28474.

920 97. Pacentine, I.V.; Nicolson, T. Subunits of the Mechano-Electrical Transduction
921 Channel, Tmc1/2b, Require Tmie to Localize in Zebrafish Sensory Hair Cells. *PLoS*
922 *Genet* **2019**, *15*, e1007635, doi:10.1371/journal.pgen.1007635.

923 98. Gopal, S.R.; Chen, D.H.-C.; Chou, S.-W.; Zang, J.; Neuhauss, S.C.F.; Stepanyan,
924 R.; McDermott, B.M.; Alagramam, K.N. Zebrafish Models for the Mechanosensory
925 Hair Cell Dysfunction in Usher Syndrome 3 Reveal That Clarin-1 Is an Essential
926 Hair Bundle Protein. *Journal of Neuroscience* **2015**, *35*, 10188–10201,
927 doi:10.1523/JNEUROSCI.1096-15.2015.

928 99. Smith, E.T.; Pacentine, I.; Shipman, A.; Hill, M.; Nicolson, T. Disruption of
929 Tmc1/2a/2b Genes in Zebrafish Reveals Subunit Requirements in Subtypes of Inner
930 Ear Hair Cells. *J Neurosci* **2020**, *40*, 4457–4468, doi:10.1523/JNEUROSCI.0163-
931 20.2020.

932 100. Chen, Z.; Chou, S.-W.; McDermott, B.M. Ribeye Protein Is Intrinsically Dynamic
933 but Is Stabilized in the Context of the Ribbon Synapse. *J Physiol* **2018**, *596*, 409–
934 421, doi:10.1113/JP271215.

935 101. Hwang, P.; Chou, S.-W.; Chen, Z.; McDermott, B.M. The Stereociliary Paracrystal
936 Is a Dynamic Cytoskeletal Scaffold In Vivo. *Cell Rep* **2015**, *13*, 1287–1294,
937 doi:10.1016/j.celrep.2015.10.003.

938 102. Sheets, L.; Hagen, M.W.; Nicolson, T. Characterization of Ribeye Subunits in
939 Zebrafish Hair Cells Reveals That Exogenous Ribeye B-Domain and CtBP1
940 Localize to the Basal Ends of Synaptic Ribbons. *PLoS One* **2014**, *9*, e107256,
941 doi:10.1371/journal.pone.0107256.

942 103. Choksi, S.P.; Babu, D.; Lau, D.; Yu, X.; Roy, S. Systematic Discovery of Novel
943 Ciliary Genes through Functional Genomics in the Zebrafish. *Development* **2014**,
944 *141*, 3410–3419, doi:10.1242/dev.108209.

945 104. Walentek, P.; Quigley, I.K.; Sun, D.I.; Sajjan, U.K.; Kintner, C.; Harland, R.M.
946 Ciliary Transcription Factors and MiRNAs Precisely Regulate Cp110 Levels
947 Required for Ciliary Adhesions and Ciliogenesis. *Elife* **2016**, *5*,
948 doi:10.7554/eLife.17557.

949 105. Stauber, M.; Weidemann, M.; Dittrich-Breiholz, O.; Lobschat, K.; Alten, L.; Mai,
950 M.; Beckers, A.; Kracht, M.; Gossler, A. Identification of FOXJ1 Effectors during
951 Ciliogenesis in the Foetal Respiratory Epithelium and Embryonic Left-Right
952 Organiser of the Mouse. *Dev Biol* **2017**, *423*, 170–188,
953 doi:10.1016/j.ydbio.2016.11.019.

954 106. Alsolami, M.; Kuhns, S.; Alsulami, M.; Blacque, O.E. ERICH3 in Primary Cilia
955 Regulates Cilium Formation and the Localisations of Ciliary Transport and Sonic
956 Hedgehog Signaling Proteins. *Scientific Reports 2019 9:1* **2019**, *9*, 1–13,
957 doi:10.1038/s41598-019-52830-1.

958 107. Imtiaz, A.; Belyantseva, I.A.; Beirl, A.J.; Fenollar-Ferrer, C.; Bashir, R.; Bukhari, I.;
959 Bouzid, A.; Shaukat, U.; Azaiez, H.; Booth, K.T.; et al. CDC14A Phosphatase Is
960 Essential for Hearing and Male Fertility in Mouse and Human. *Hum Mol Genet* **2018**,
961 *27*, 780–798, doi:10.1093/hmg/ddx440.

962 108. Schwenk, B.M.; Lang, C.M.; Hogl, S.; Tahirovic, S.; Orozco, D.; Rentzsch, K.;
963 Lichtenthaler, S.F.; Hoogenraad, C.C.; Capell, A.; Haass, C.; et al. The FTLD Risk
964 Factor TMEM106B and MAP6 Control Dendritic Trafficking of Lysosomes. *EMBO*
965 *J* **2013**, *33*, n/a-n/a, doi:10.1002/embj.201385857.

966 109. Gory-Fauré, S.; Windscheid, V.; Brocard, J.; Montessuit, S.; Tsutsumi, R.; Denarier,
967 E.; Fukata, Y.; Bosc, C.; Delaroche, J.; Collomb, N.; et al. Non-Microtubular
968 Localizations of Microtubule-Associated Protein 6 (MAP6). *PLoS One* **2014**, *9*,
969 e114905, doi:10.1371/journal.pone.0114905.

970 110. Tortosa, E.; Adolfs, Y.; Fukata, M.; Pasterkamp, R.J.; Kapitein, L.C.; Hoogenraad,
971 C.C. Dynamic Palmitoylation Targets MAP6 to the Axon to Promote Microtubule
972 Stabilization during Neuronal Polarization. *Neuron* **2017**, *94*, 809-825.e7,
973 doi:10.1016/j.neuron.2017.04.042.

974 111. Lu, Q.; Insinna, C.; Ott, C.; Stauffer, J.; Pintado, P.A.; Rahajeng, J.; Baxa, U.; Walia,
975 V.; Cuenca, A.; Hwang, Y.S.; et al. Early Steps in Primary Cilium Assembly Require
976 EHD1/EHD3-Dependent Ciliary Vesicle Formation. *Nature Cell Biology 2014 17:3*
977 **2015**, *17*, 228–240, doi:10.1038/ncb3109.

978 112. Lee, J.; Chung, Y.D. Ciliary Subcompartments: How Are They Established and
979 What Are Their Functions? *BMB Rep* **2015**, *48*, 380–387,
980 doi:10.5483/BMBRep.2015.48.7.084.

981 113. Gui, M.; Farley, H.; Anujan, P.; Anderson, J.R.; Maxwell, D.W.; Whitchurch, J.B.;
982 Botsch, J.J.; Qiu, T.; Meleppattu, S.; Singh, S.K.; et al. De Novo Identification of
983 Mammalian Ciliary Motility Proteins Using Cryo-EM. *Cell* **2021**, *184*, 5791-
984 5806.e19, doi:10.1016/j.cell.2021.10.007.

985 114. Lagziel, A.; Ahmed, Z.M.; Schultz, J.M.; Morell, R.J.; Belyantseva, I.A.; Friedman,
986 T.B. Spatiotemporal Pattern and Isoforms of Cadherin 23 in Wild Type and Waltzer
987 Mice during Inner Ear Hair Cell Development. *Dev Biol* **2005**, *280*, 295–306,
988 doi:10.1016/j.ydbio.2005.01.015.

989 115. Nicolson, T.; Rüsch, A.; Friedrich, R.W.; Granato, M.; Ruppersberg, J.P.; Nüsslein-
990 Volhard, C. Genetic Analysis of Vertebrate Sensory Hair Cell Mechanosensation:

The Zebrafish Circler Mutants. *Neuron* **1998**, *20*, 271–283, doi:10.1016/S0896-6273(00)80455-9.

116. Lanford, P.J.; Lan, Y.; Jiang, R.; Lindsell, C.; Weinmaster, G.; Gridley, T.; Kelley, M.W. Notch Signalling Pathway Mediates Hair Cell Development in Mammalian Cochlea. *Nature Genetics 1999 21:3* **1999**, *21*, 289–292, doi:10.1038/6804.

117. Zine, A.; van de Water, T.R.; de Ribaupierre, F. Notch Signaling Regulates the Pattern of Auditory Hair Cell Differentiation in Mammals. *Development* **2000**, *127*, 3373–3383, doi:10.1242/dev.127.15.3373.

118. Bowl, M.R.; Brown, S.D.M. Genetic Landscape of Auditory Dysfunction. *Hum Mol Genet* **2018**, *27*, R130–R135, doi:10.1093/hmg/ddy158.

119. Groza, T.; Gomez, F.L.; Mashhadi, H.H.; Muñoz-Fuentes, V.; Gunes, O.; Wilson, R.; Cacheiro, P.; Frost, A.; Keskivali-Bond, P.; Vardal, B.; et al. The International Mouse Phenotyping Consortium: Comprehensive Knockout Phenotyping Underpinning the Study of Human Disease. *Nucleic Acids Res* **2022**, doi:10.1093/nar/gkac972.

120. Kolla, L.; Kelly, M.C.; Mann, Z.F.; Anaya-Rocha, A.; Ellis, K.; Lemons, A.; Palermo, A.T.; So, K.S.; Mays, J.C.; Orvis, J.; et al. Characterization of the Development of the Mouse Cochlear Epithelium at the Single Cell Level. *Nature Communications 2020 11:1* **2020**, *11*, 1–16, doi:10.1038/s41467-020-16113-y.

121. Kubota, M.; Scheibinger, M.; Jan, T.A.; Heller, S. Greater Epithelial Ridge Cells Are the Principal Organoid-Forming Progenitors of the Mouse Cochlea. *Cell Rep* **2021**, *34*, 108646, doi:10.1016/j.celrep.2020.108646.

122. Steiner, A.B.; Kim, T.; Cabot, V.; Hudspeth, A.J. Dynamic Gene Expression by Putative Hair-Cell Progenitors during Regeneration in the Zebrafish Lateral Line. *Proc Natl Acad Sci U S A* **2014**, *111*, E1393-401, doi:10.1073/pnas.1318692111.

123. Liu, Y.; Pathak, N.; Kramer-Zucker, A.; Drummond, I.A. Notch Signaling Controls the Differentiation of Transporting Epithelia and Multiciliated Cells in the Zebrafish Pronephros. *Development* **2007**, *134*, 1111–1122, doi:10.1242/dev.02806.

124. Hsu, C.-C.; Hou, M.-F.; Hong, J.-R.; Wu, J.-L.; Her, G.M. Inducible Male Infertility by Targeted Cell Ablation in Zebrafish Testis. *Mar Biotechnol (NY)* **2010**, *12*, 466–478, doi:10.1007/s10126-009-9248-4.

1024

7. Figures

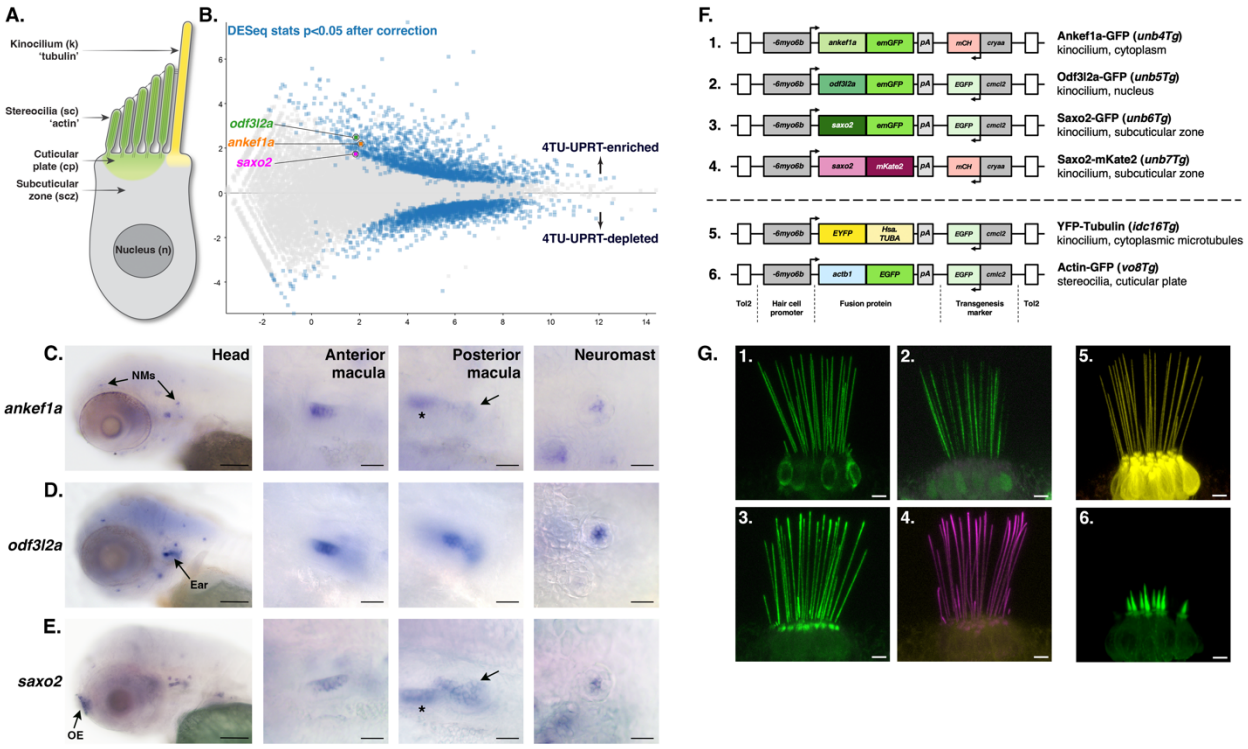

Figure 1. Identification of cilium-associated genes with enriched expression in zebrafish hair cells. **A.** Diagram of a generic sensory hair cell. **B.** Scatter plot of differentially expressed genes identified by TU-tagging. *ankef1a*, *odf3l2a*, and *saxo2* are indicated in the 4TU-UPRT-enriched population. **C-E.** mRNA in situ hybridization (ISH) for *ankef1a*, *odf3l2a* and *saxo2* in 3 days post-fertilization (dpf) zebrafish larvae. NMs = neuromasts; OE = olfactory epithelium. In the *ankef1a* and *saxo2* posterior macula panels, arrows point to the posterior macula sensory patch while the asterisk indicates the out of focus anterior macula. **F.** Schematic of transgenic genes used in this study. **G.** Overview of Ankef1a-GFP (1), Odf3l2a-GFP (2), Saxo2-GFP (3), Saxo2-mKate2 (4), YFP-TUBA (5), and Actb1-GFP (6) protein localization in the lateral cristae of larval zebrafish. Scale bars are 100 µm for the head shots in C-E, 20 µm for all other ISH panels. Scale bars are 5 µm in G.

1025

1026

1027

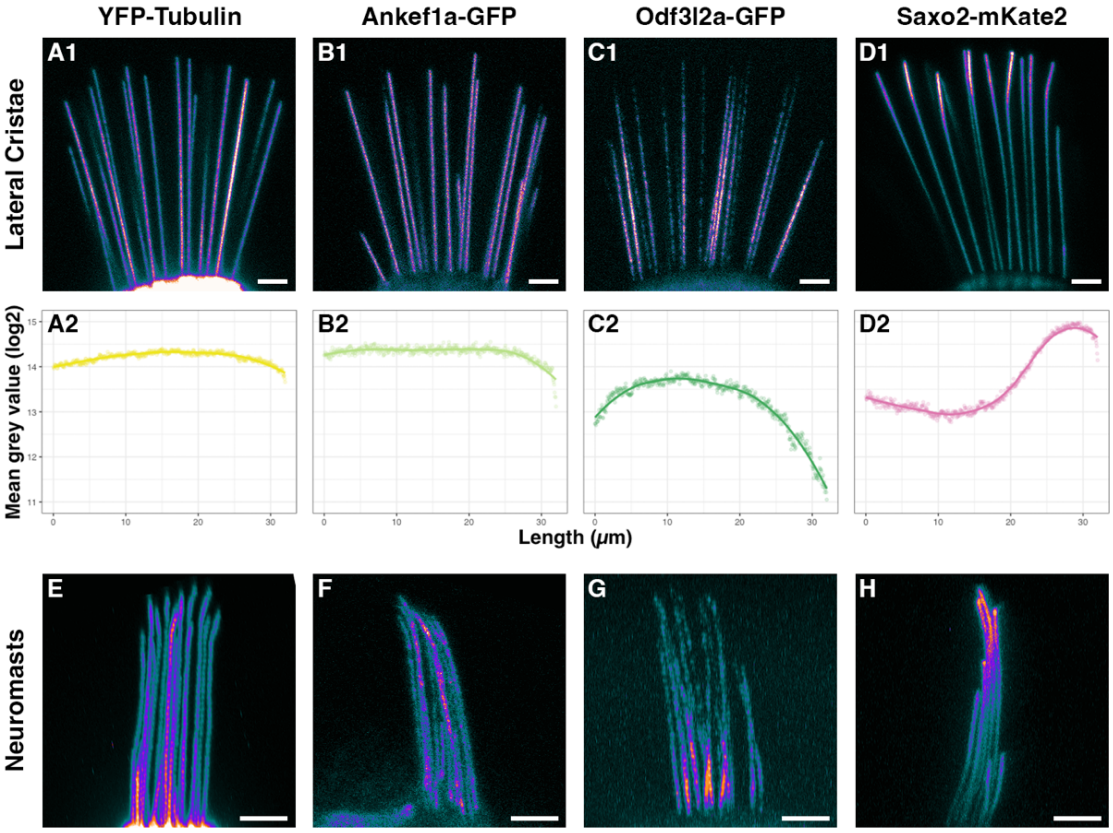

Figure 2. Distributions of tubulin, Ankef1a, Odf3l2a, and Saxo2 in the hair cell kinocilium. **A1 – D1.** Pixel intensity-encoded images of tagged alpha tubulin, Ankef1a, Odf3l2a, and Saxo2 proteins in the kinocilia of lateral cristae hair cells. Brighter colours indicate higher fluorescence intensity. **A2 – D2.** Scatter plots of averaged mean grey values (log2) for fluorescence intensity from kinocilia in the lateral cristae of YFP-TUBA (n = 35 kinocilia from 8 individuals), Ankef1a-GFP (n = 23 from 8 individuals), Odf3l2a-GFP (n = 30 from 11 individuals), and Saxo2-mKate2 (n = 17 from 6 individuals). Position 0 µm is from the proximal region near the base of kinocilia and position 32 µm is the distal-most tip. **E – H.** Pixel intensity-encoded images of neuromast kinocilia from YFP-TUBA, Ankef1a-GFP, Odf3l2a-GFP, and Saxo2-mKate2 expressing zebrafish larvae. Scale bars are 5 µm in panels A1-D1, E-H.

1028

1029

1030

1031

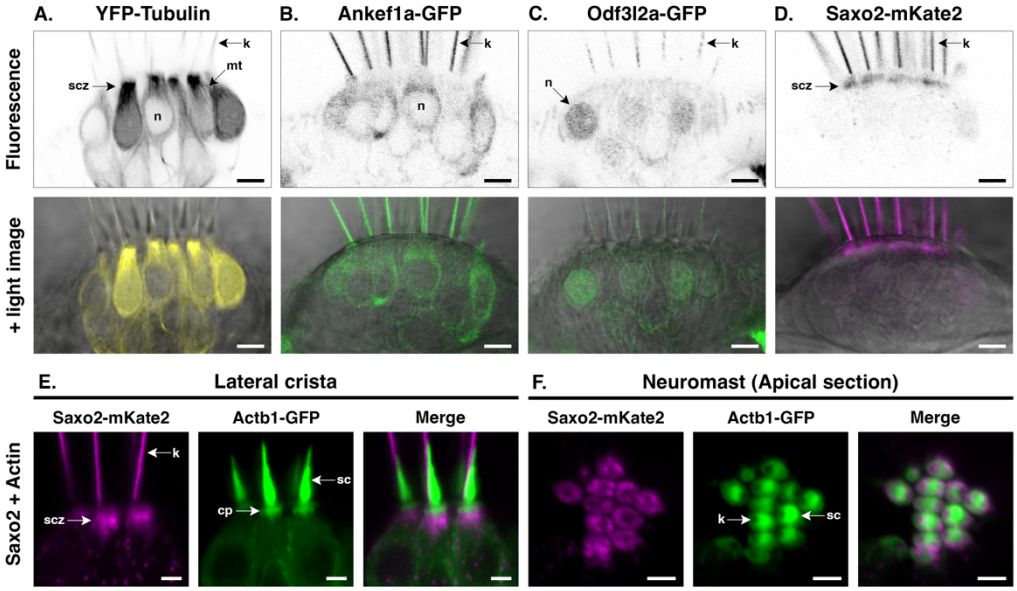

Figure 3. Distinct protein localization patterns in the hair cell soma. **A – D.** Details of YFP-TUBA, Ankef1a-GFP, Odf3l2a-GFP, and Saxo2-mKate2 in the hair cell body. Top panels are black and white representations of the fluorescence channel and lower panels are fluorescence with the corresponding light image. **E, F.** Saxo2-mKate2 (magenta) accumulations in apical part of the hair cell body in cristae and neuromasts. GFP-tagged beta actin is shown in green. scz = subcuticular zone; mt = microtubule; k = kinocilium; n = nucleus; cp = cuticular plate; sc = stereocilia. Scale bars are 5 µm in A – D and 2.5 µm in E and F.

1032

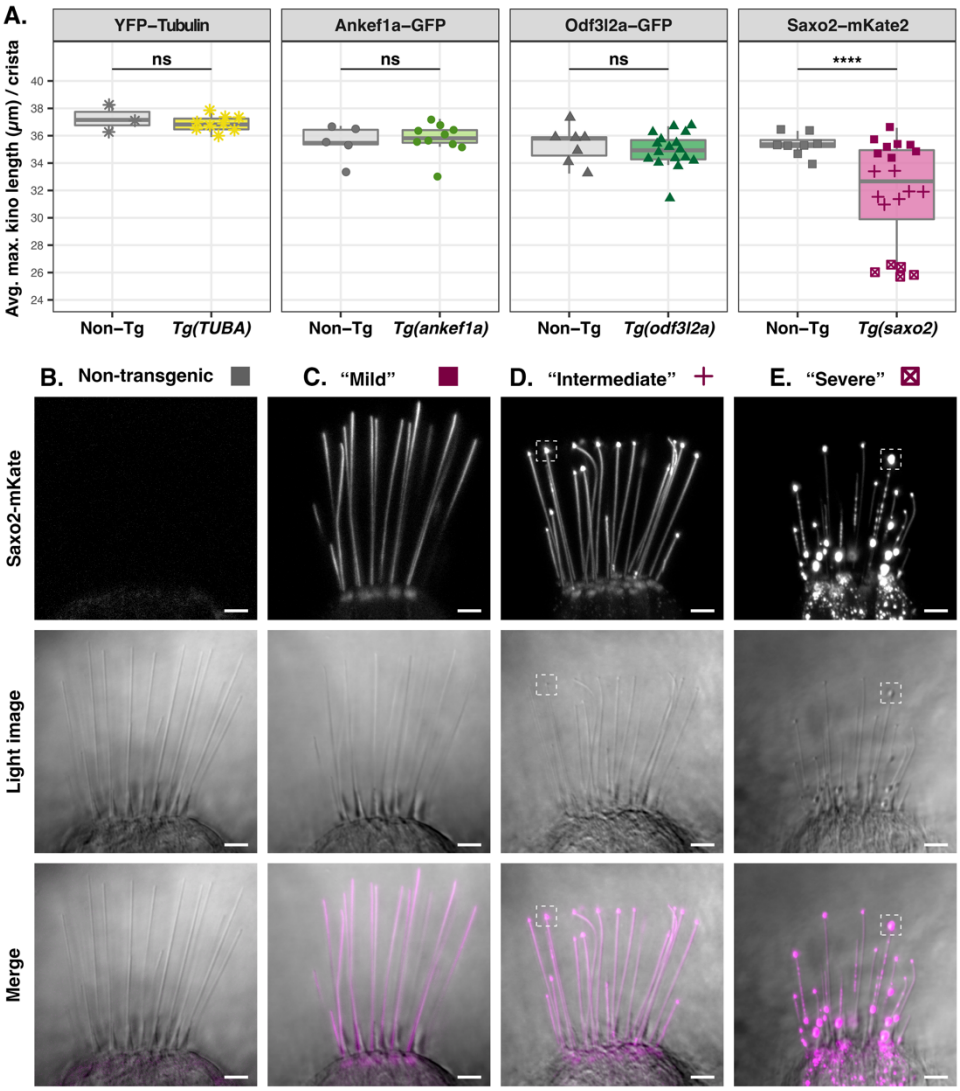

Figure 4. Effect of tubulin, Ankef1a, Odf3l2a, and Saxo2 overexpression on kinocilial length and morphology. **A.** Boxplots of maximum kinocilia length in the lateral crista of *YFP-TUBA*, *ankef1a-GFP*, *odf3l2a-GFP*, and *saxo2-mKate2* transgenics and their non-transgenic siblings. Data points are the average length of the five tallest kinocilia from an individual larva. Based on their morphological phenotypes, the Saxo2-mKate2 data points are grouped as "mild" (solid squares), "intermediate" (crosses), and "severe" (boxed x's). Two-tailed Welch's t-test statistics - YFP-tubulin (6 dpf): non-Tg, n = 3 larvae, mean = 37.3 µm; *Tg(TUBA)*, n = 9, mean = 36.9 µm; t = 0.67757, df = 2.5116, p = 0.5551. Ankef1a-GFP (5 dpf): non-Tg, n = 5, mean = 35.5 µm; *Tg(ankef1a)*, n = 10, mean = 35.7 µm; t = 0.41384, df = 7.079, p = 0.6912. Odf3l2a-GFP (5 dpf): non-Tg, n = 7, mean = 35.3 µm; *Tg(odf3l2a)*, n = 17, mean = 35.0 µm; t = 0.5913, df = 10.931, p = 0.5663. Saxo2-mKate2 (5 dpf) one-way ANOVA ($F_{3,24}$ = 193.3, p < 2e-16). See text for results of pairwise comparisons between the Saxo2-mKate2 phenotypes. **B - E.** Representative images of lateral cristae from non-transgenic (B) and *saxo2-mKate2* transgenics categorized as "mild" (C), "intermediate" (D), and "severe" (E). The dashed boxes in D and E highlight examples of the "bulbed" kinocilial phenotype. ns = not significant; **** = p < 0.00001. Scale bars are 5 µm.

1033

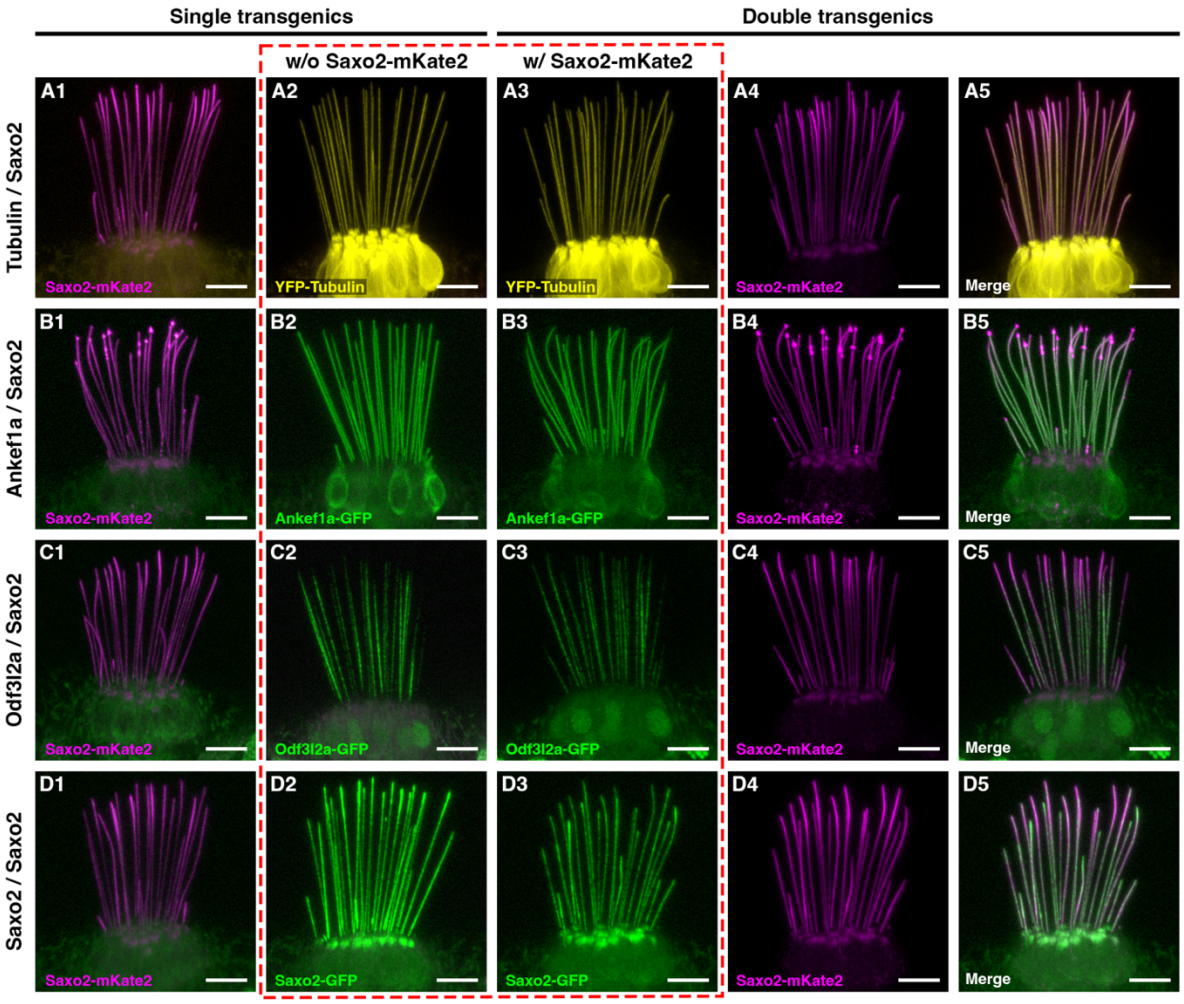

Figure 5. Co-expression of Saxo2-mKate2 with YFP-tubulin (**A**), Ankef1a-GFP (**B**), Odf3l2a-GFP (**C**), and Saxo2-GFP (**D**). Column 1 and 2 of each row shows single transgenic siblings while columns 3 and 4 show individual channels from a double transgenic larva. Column 5 shows the merged channels from columns 3 and 4. The dashed red box compares YFP-TUBA, Ankef1a-GFP, Odf3l2a-GFP, and Saxo2-GFP localization without (A2-D2) or with (A3-D3) the presence of Saxo2-mKate2. Scale bars are 5 µm in all panels.

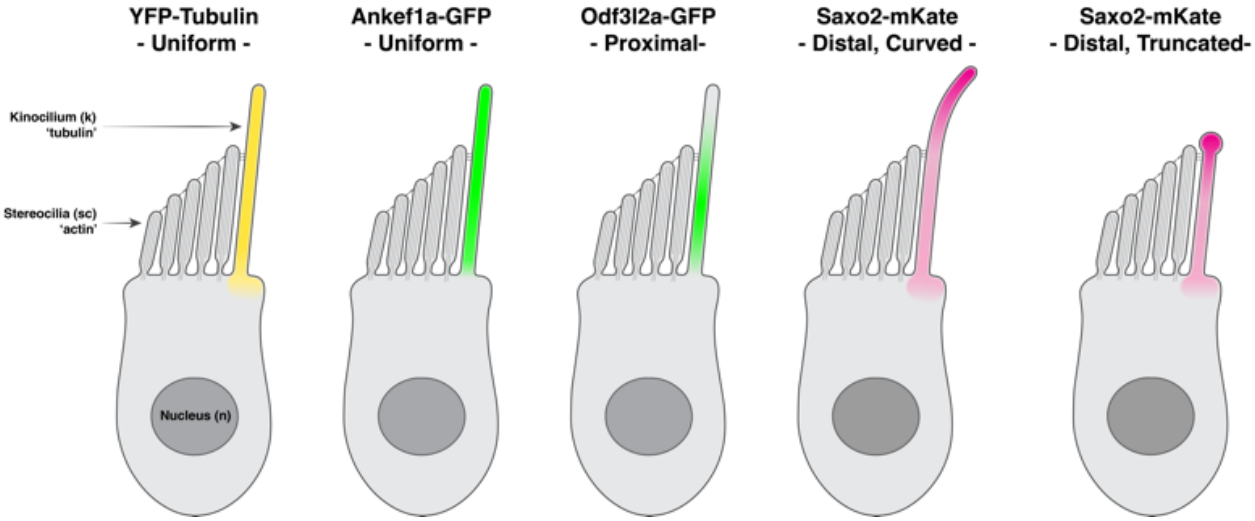

Figure 6. Summary of kinocilial localization patterns and phenotypes for Ankef1a, Odf3l2a, and Saxo2.

1038

1039

1040

1041

Table 1: Human *ANKEF1*, *ODF3L2*, and *SAXO2* chromosomal locations compared to potential associated deafness loci.

Human gene	Cytogenetic Location	GRCh38.p13 coordinates	Proposed deafness locus	Critical region markers	Locus coordinates	Causative gene	Reference
ANKEF1	20p12.2	20:10034987-10058303	n/a	n/a	n/a	n/a	n/a
ODF3L2	19p13.3	19:463346-474880	*DFNB72*	D19S216 - D19S1034	19:4949401-6113471	*GIPC3*	Ain et al. [73]
			DFNA57	D19S912 - D19S212	19:7806762 - 18232460	unknown	Bönsch et al. [72]
SAXO2	15q25.2	15:82262818-82284927	*DFNA30*	D15S151 - D15S130	15:87053920-94168232	unknown	Mangino et al. [85]

1042

1043

1044

8. Supplemental Figures

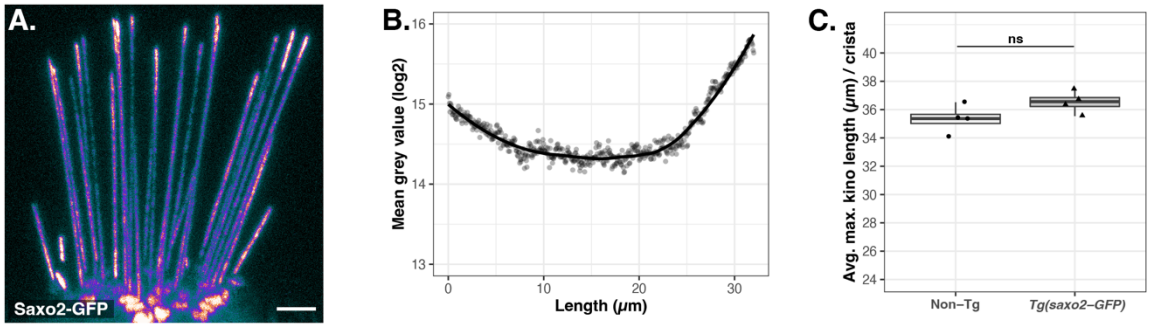

Figure S1. Saxo2-GFP kinocilial distribution and effect on kinocilia height. **A.** Pixel intensity-encoded image of Saxo2-GFP in the kinocilia of lateral cristae hair cells. Brighter colours indicate higher fluorescence intensity. **B.** Scatter plot of averaged mean grey values (log2) for fluorescence intensity from kinocilia in the lateral cristae of 5 dpf Saxo2-GFP transgenics (n = 16 kinocilia from 4 individuals). Position 0 µm is from the proximal region near the base of kinocilia and position 32 µm is the distal-most tip. **C.** Boxplots of maximum kinocilia length in the lateral crista of 5 dpf *saxo2-GFP* transgenics and their non-transgenic siblings. Data points are the average length of the five tallest kinocilia from an individual larva. Two-tailed Welch's t-test statistics: non-Tg, n = 4 larvae, mean = 35.3 µm; *Tg(saxo2-GFP)*, n = 4, mean = 36.5 µm; t = -1.8712, df = 5.5674, p = 0.1143. Scale bar is 5 µm in A.

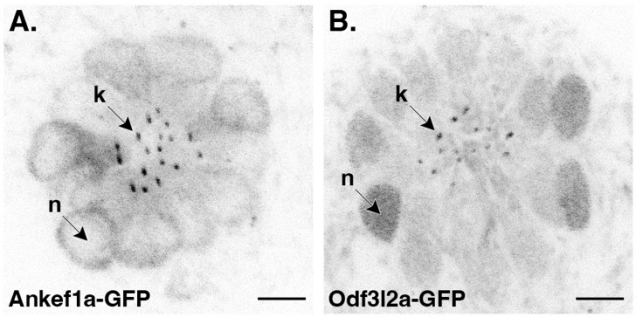

Figure S2. Ankef1a-GFP (**A**) and Odf3l2a-GFP (**B**) localization patterns in the soma of neuromast hair cells (top-down views). n = nucleus, k = kinocilium. Scale bars are 5 µm.

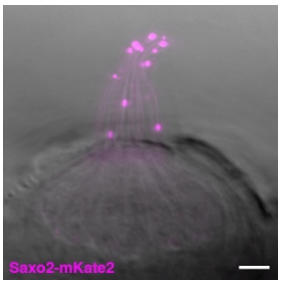

Figure S3. An example of truncated and bulbed kinocilia in the neuromasts of *saxo2-mKate2* transgenics with the "severe" overexpression phenotype. Scale bar is 5 µm.

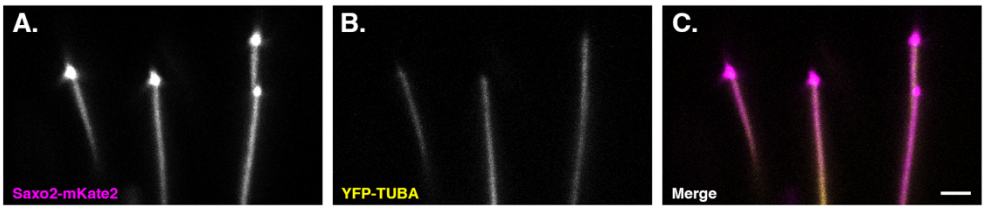

Figure S4. Detail of Saxo2-mKate2 (**A**) and YFP-TUBA (**B**) co-expression at the distal tip of kinocilia in the lateral cristae. Merged channels are shown in C. Scale bar is 2 µm.

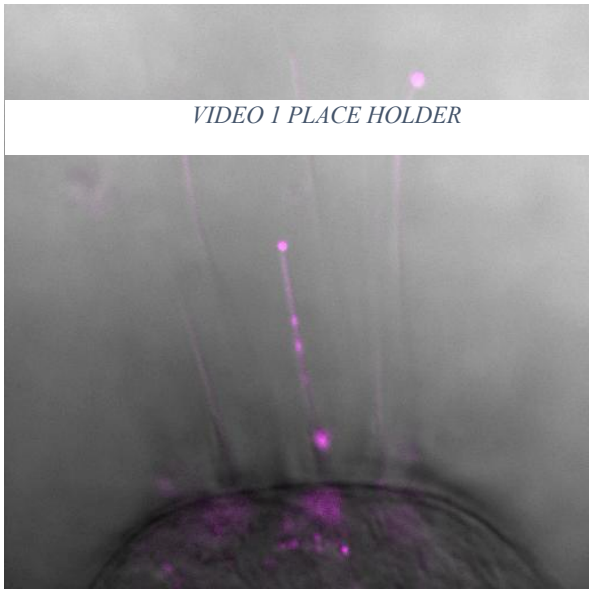

Video S1. Bidirectional movement of a Saxo2-mKate2 positive puncta in the kinocilium of a lateral crista hair cell in a 5 dpf zebrafish larva.